Materials Horizons

ROYAL SOCIETY OF CHEMISTRY

REVIEW

View Article Online
View Journal | View Issue

Cite this: *Mater. Horiz.*, 2024, **11**, 5843

A review of advanced helical fibers: formation mechanism, preparation, properties, and applications

Minmin Ding,[a] Xiuling Yang,[a] Yanbo Liu,*[b] Shiyi Zeng,[a] Gaigai Duan,*[a] Yong Huang,[a] Zhao Liang,*[c] Peng Zhang,[d] Jian Ji[d] and Shaohua Jiang*[a]

Received 11th June 2024,
Accepted 14th August 2024

DOI: 10.1039/d4mh00737a

rsc.li/materials-horizons

As a unique structural form, helical structures have a wide range of application prospects. In the field of biology, helical structures are essential for the function of biological macromolecules such as proteins, so the study of helical structures can help to deeply understand life phenomena and develop new biotechnology. In materials science, helical structures can give rise to special physical and chemical properties, such as in the case of spiral nanotubes, helical fibers, *etc.*, which are expected to be used in energy, environment, medical and other fields. The helical structure also has unique charm and application value in the fields of aesthetics and architecture. In addition, helical fibers have attracted a lot of attention because of their tendrils' vascular geometry and indispensable structural properties. In this paper, the development of helical fibers is briefly reviewed from the aspects of mechanism, synthesis process and application. Due to their good chemical and physical properties, helical fibers have a good application prospect in many fields. Potential problems and future opportunities for helical fibers are also presented for future studies.

Wider impact

What key developments in the field of research are discussed?
This review discusses some of the key developments in helical fibers in mimicking biological structures, optimizing performance, and expanding applications.
What makes the field of study broadly meaningful?
Helical fibers have made significant progress in many areas, for example, in biomedical and tissue engineering, where artificial skin can be prepared. But there are still some challenges and problems that need to be solved, and this article happens to discuss the current state of helical fibers, and the advantages and disadvantages of helical fibers, and provide some solutions to the problems that affect the broader development of helical fibers.
What does the future hold for the field, and how will the insights from this review help shape materials science?
As a material with special structure and excellent properties, the future development of spiral fiber will be affected by many factors, including scientific and technological progress, market demand and the expansion of application fields. The article provides some ways to further develop it, such as further improving production efficiency, reducing costs, and optimizing performance. In the future, with the continuous progress of science and technology and the increasing demand for high-performance materials, the development prospect of spiral fiber will be broader.

1. Introduction

Helical structures are ubiquitous in nature, from microscopic DNA, bacterial flagella, and viral capsid to macroscopic seed pods and plant tendrils. The term spiral structure first appeared in 1953, when Davis *et al.* discovered that there were spiral-shaped structures in carbon vermicides, and after stereoscopic examination, this structure was found to be composed of many thicker threads that were wrapped together in the form of ropes.[1] Helical structures can be found in nature at various length scales ranging from the molecular level to the macroscale. Due to their ability to store mechanical energy and to optimize the accessible surface

[a] *Jiangsu Co-Innovation Center of Efficient Processing and Utilization of Forest Resources, International Innovation Center for Forest Chemicals and Materials, College of Materials Science and Engineering, Nanjing Forestry University, Nanjing, 210037, China. E-mail: duangaigai@njfu.edu.cn, shaohua.jiang@njfu.edu.cn*
[b] *State Key Laboratory of New Textile Materials and Advanced Processing Technologies, School of Textile Science and Engineering, Wuhan Textile University, Wuhan, 430200, China. E-mail: yanboliu@gmail.com*
[c] *Institute of Micro/Nano Materials and Devices, Ningbo University of Technology, Ningbo, 315211, Zhejiang, China. E-mail: walleliang@hun.edu.cn*
[d] *MOE Key Laboratory of Macromolecule Synthesis and Functionalization, Department of Polymer Science and Engineering, Zhejiang University, Hangzhou, China*

area, helical shapes contribute particularly to motion-driven processes and structural reinforcement.[2]

In the past ten years, with the rise and development of nanotechnology, nanofibers with smaller diameter and finer structure have been developed, which has greatly expanded the research and application of biomimetic material design, and biomimetic material design has attracted extensive attention from academia and industry. As a low-dimensional nanostructure, micro/nanofiber has unique properties, for example, adjustable structure, high specific surface area, excellent mechanical properties, and so on. Inspired by the helical structure in nature, the helical fiber is widely favored. Many groups have proposed methods to produce helical fibers, including mechanical twisting,[2–4] chemical deposition,[5] microfluidics,[5,6] and electrospinning.[7–11] The helical micro–nanofiber formed by introducing the helical structure into micro/nanofiber still maintains the high mechanical properties of the fiber. Additionally, the presence of the helical structure not only improves the porosity of the fibrous material, but also adds some excellent properties: (1) it provides good mechanical properties, especially elasticity and flexibility, (2) the three-dimensional spiral structure allows the fiber to have more degrees of freedom and can provide a larger specific surface area, and (3) the fiber aggregate has more support cavities and higher porosity. Due to the excellent properties brought about by the helical structure, spiral micro–nanofibers have important application prospects in the fields of adsorption filtration,[12] thermal insulation materials,[13] tissue engineering,[14] micro–nano electromechanical systems,[15] microelectronic components,[16] and so on.

Due to the special structure of the helical fibers, the helical fibers maintain a uniform stress distribution even when fully stretched. Additionally, the stretchable helical fibers return to their original shape completely even after being fully compressed vertically. Therefore, the application in stretchability also shows broad prospects.[17] In addition, the length, diameter and pitch of the spiral microfibers can be highly controlled. For example, changing the injection capillary design of microfluidics in microfluidic spinning can produce spiral microfibers with new Janus, triple, core–shell and even double helical structures. The potential use of these helical microfibers has also been explored for magnetic and thermodynamically triggered microsprings, as well as force indicators of cardiomyocyte contraction. This shows that this spiral microfiber is highly versatile in different applications.[6] Although there are many research articles published on the preparation of helical fibers and their applications, it is necessary to summarize the advanced developments of the helical fibers. Therefore, this paper comprehensively summarizes the methods and principles of helical fibers, and finally analyzes the applications of various helical fibers in various fields (Fig. 1).

2. Formation mechanism of helical fibers

The formation mechanism of spiral fibers has important research value in different fields, such as textiles, materials science and biology. For example, through composite electrospinning and two-component melt blown spinning process, the required helical structure is obtained by using the performance differences between different polymers, which highlights the original properties and gives them elasticity and flexibility, which has important application prospects in the fields of adsorption filtration,[30] micro–nano electromechanical systems[15] and microelectronic components.[31] Or through the chemical vapor deposition method (CVD method), with nickel as the catalyst, acetylene as the carbon source, and sulfur-containing compounds as the co-catalyst, with the reaction temperature at 700–850 °C, spiral carbon fibers with different spiral diameters can be prepared.[30–33] From this point of view, the current state of affairs is to study the formation of helical fibers, so this section summarizes several mechanisms for the formation of helical fibers, such as catalytic cracking of certain substances; the properties of the fibers themselves.[34,35]

2.1. Construction of helical structure by responsivity

Responsive helical fibers are a class of fiber materials with special response characteristics, which can sense and respond to changes in the external environment, such as temperature, light, magnetic field, *etc.*, and then produce changes in morphology, physical properties or chemical properties. This responsiveness makes responsive helical fibers have a wide range of application prospects in smart materials, biomedicine, environmental science, and other fields.

2.1.1. Magnetically triggered helical coil construction. The magnetically responsive helical fiber is a special type of fibrous material that is able to produce a response under the action of an external magnetic field and exhibit corresponding physical changes. This fiber typically achieves its magnetic responsiveness owing to the magnetic nanoparticles embedded or loaded inside the fiber. When a magnetically responsive helical fiber is placed in an external magnetic field, the magnetic nanoparticles inside the fiber are subjected to a magnetic force, resulting in a change in the overall shape or arrangement of the fiber.[36] Huang *et al.* developed helical coil structures for drive applications by magnetic drives.[37] Here they developed an origami-inspired rapid prototyping process for building self-folding, magnetically powered micromachines with complex body plans, reconfigurable shape and controllable motility. Selective reprogramming of the mechanical design and magnetic anisotropy of body parts dynamically modulates the swimming characteristics of the micromachines. They found that tail and body morphologies together determine swimming efficiency and, unlike for rigid swimmers, the choice of magnetic field can subtly change the motility of soft microswimmers. This structure consists of a non-swelling support hydrogel layer composed of poly(ethylene glycol) diacrylate (PEGDA) that is selectively patterned on a swelling thermally responsive *N*-isopropylacrylamide (NIPAm) hydrogel layer. The movement of these devices is induced by the addition of magnetic nanoparticles (MNPs) to the hydrogel layer and customized by magnetically arranging the particles during polymerization. Fig. 2a and b illustrates the realization of a soft micro-machine with programmable motion and morphology through the control of MNPs.

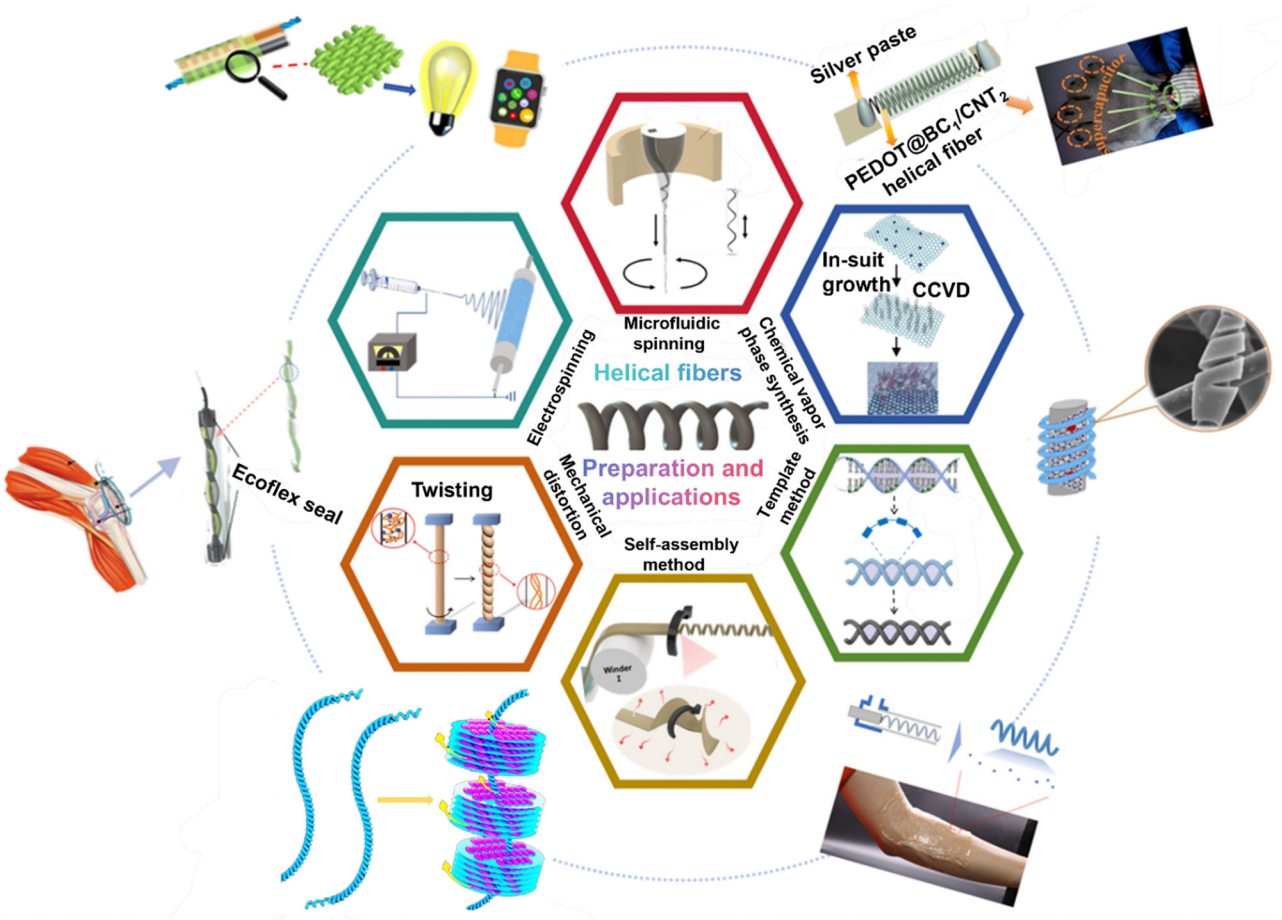

Fig. 1 Preparation methods and applications of helical fibers. Reproduced with permission,[18] Copyright © 2024, The Author(s); reproduced with permission,[19] © 2022 The Authors. Publishing services by Elsevier B.V. on behalf of KeAi Communications Co. Ltd; reproduced with permission,[20] Copyright © 2023 The Authors. Published by American Chemical Society; reproduced with permission,[21] © 2023 Wiley-VCH GmbH; reproduced with permission,[22] © 2024 Wiley-VCH GmbH; reproduced with permission,[23] © 2023 Elsevier B.V. All rights reserved; reproduced with permission,[24] © 2021 Elsevier Ltd. All rights reserved; reproduced with permission,[25] Copyright © 2022 American Chemical Society; reproduced with permission,[26] Copyright © 2021 American Chemical Society; reproduced with permission,[27] © 2022 Wiley Periodicals LLC; reproduced with permission,[28] © 2021 Elsevier B.V. All rights reserved; reproduced with permission,[29] © 2021 Elsevier B.V. All rights reserved.

2.1.2. Helical construction by thermoresponse. Thermally responsive materials have been widely applied in different research areas, such as drug delivery,[40–42] actuation,[43,44] and so on. The thermally responsive helical fiber is a spiral-shaped

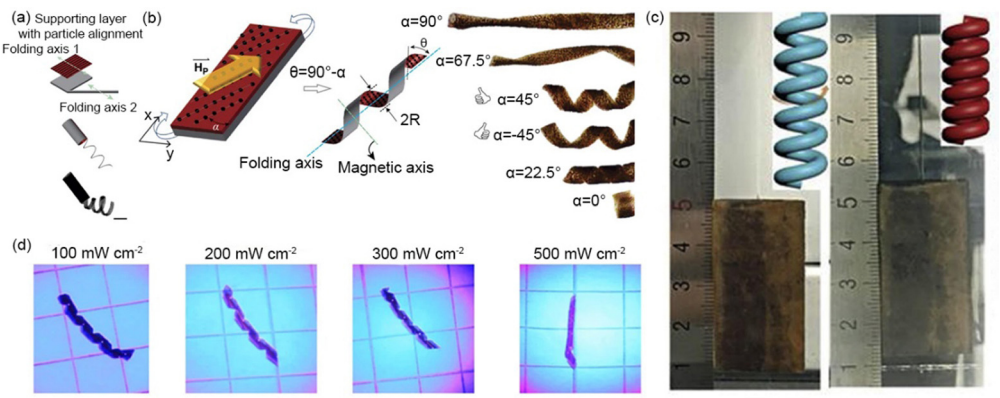

Fig. 2 The final three-dimensional shape of the helical structure with (a) bilayer and (b) monolayer hydrogels after autonomous folding is controlled by the alignment of the embedded MNPs,[37] © 2024 Springer Nature Limited; (c) CPY photos before (left) and after heating (right) at 180 °C,[38] © 2019 Elsevier B.V. All rights reserved; (d) representative images of azo-LCN bands in the range of light intensity from 100 to 500 mW cm^{-2},[39] © 2024 Springer Nature Limited.

fibrous material that is able to respond to temperature changes and exhibit corresponding physical changes. Such fibers are typically prepared based on heat-sensitive materials that undergo changes in physical or chemical properties when temperature changes, altering the morphology or properties of the fibers.[45] Huang *et al.* demonstrated a novel layered structure and multi-response actuator by twisting electro-spun polyamide-6 into a coiled yarn (CPY).[38] Due to the presence of microscale and nanoscale cavities, CPY can reversibly rotate in response to various organic solvents, and the rotation speed depends on the type of solvent. Capillary force-driven contraction is thought to be the driving mechanism of our CPY, and it is different from all previously reported wound yarns. The high coefficient of thermal expansion of polyamide-6 also makes CPY thermally responsive, as CPY exhibits contraction when heated due to untwisting due to volume expansion (Fig. 2c). This actuator, which is capable of mechanically reacting to external stimuli, has great potential for application in artificial muscles, soft robots, sensors, generators, and more.

2.1.3. Light-responsive helix formation. The light-responsive helical fiber is a spiral-shaped fibrous material that is able to respond to light and exhibit specific physical or chemical changes. These fibers usually respond to light owing to photosensitizing substances or structures introduced into the fibers. Jeong *et al.* discovered light-induced motion (photo motion) in monolithic polymer films prepared based on azobenzene functionalized liquid crystal polymer networks (azo-LCN).[39] The film is transformed from a flat plate to a helical band by illumination with broad-spectrum UV-Vis light (320–500 nm) in a twisted nematic direction, followed by continuous irradiation over a long distance on any surface. This movement is caused by a complex interaction of photochemistry and mechanics and demonstrates direction control as well as climbing. Fig. 2d illustrates the photoinduced motion (photo kinesis) of thin strips of light-responsive polymers that transform from flat to helical structures upon irradiation. This monolithic and light-responsive polymer material is an azo-LCN composed of 20 wt% azobenzene crosslinker.[46] Photo kinetics is the spontaneous mechanical response of these anisotropic materials, where the intrinsic particle size of the driving mechanism is at the molecular level (*trans–cis*-isomerization) and provides a fine modularity level for tuning the mechanical suitability. Zhang *et al.* designed and developed a strategy for luminescent cholesterol liquid crystal elastomer (Lumin-CLCE) films with mechanically tuneable circularly polarized luminescence (CPL), and then achieved control of CPL intensity and direction of rotation by controlling the chirality of the self-assembled spiral nanostructure and the soft helix.[47] A major breakthrough is the implementation of a reversible, mechanically adjustable, perovskite-based CPL switch that is activated by biaxial stretching, enabling flexible, dynamic security tags to decrypt preset information at specific polarization states.

2.2. Helical fibers composed of physical factors

The mechanism of forming helical fibers by mechanical twisting mainly involves the rotational force generated in the twisting process to produce spiral torsional deformation of the fibers. During twisting, the two cross-sections of the fibers rotate relative to each other, and the fibers, which were originally parallel to the spool, tilt and form a spiral. This slanted spiral twist causes the fibers to twist and deform, allowing the yarn to hold tightly together. This change not only changes the structural morphology of the fiber collective, but also affects its mechanophysical properties. Fig. 3 illustrates the formation of bacterial cellulose (BC) and sodium alginate (Alg) multi-level helical fibers by twisting.[48]

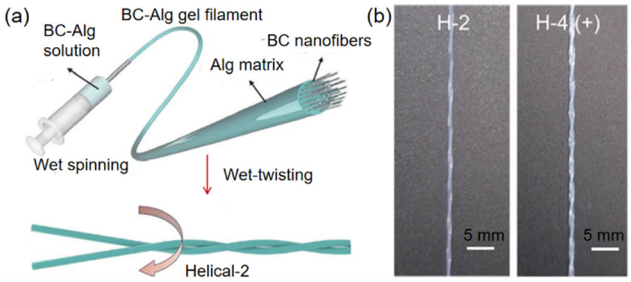

Fig. 3 The manufacturing process of multi-stage spiral BC-Alg large fibers. (a) Preparation of biomimetic layered spiral BC-Alg large fibers, two gel filaments twisted together; (b) the photograph shows the twisted state of a bundle of BC-Alg gel filaments after the wet twisting process at each layering level. Reproduced with permission,[48] Copyright © 2019, © The Author(s) 2019. Published by Oxford University Press on behalf of China Science Publishing & Media Ltd.

Therefore, the mechanism of forming helical fibers by mechanical twisting involves the rotational force generated by twisting to make the fibers produce spiral torsional deformation, so as to obtain helical fibers with specific structures and properties.

2.3. Helical fibers formed by spinning

The methods of preparing helical fibers by spinning technology include electrospinning,[49] wet spinning,[50] melt-blown spinning[51] and other methods. Electrospinning is a simple and versatile technique that can produce microfibers and nanofibers with many different helix shapes. Electrospinning is the process of stretching a polymer solution into nanofibers by applying a high-voltage electric field. The method of electrospinning has been applied to prepare helical fibers. When the polymer solution is gradually extruded according to the set flow rate, Taylor cones are formed at the outlet of the syringe due to surface tension and high electric field forces. As the voltage gradually rises to critical values, the polymer droplets break through the surface tension and form a thin stream ejected from the tip of the cone. The main mechanisms of the helical fibers obtained by electrospinning are as follows: (1) two or more polymers with different mechanical properties that can produce shrinkage/elastic stress differences in fibers are used as precursors for spinning (Fig. 4a); (2) the bending instability of the jet (including the bending instability and mechanical buckling instability when it collides with the receiving plate). Fig. 4b illustrates the process of preparing helical fibers for use in an air purifier by electro-blowing.

In addition to the use of multiple components, it is also possible to spin a single polymer; for example, using only one polypropylene polymer (PP) with different melt flow rate (MFR) as two components, by adjusting the processing conditions,

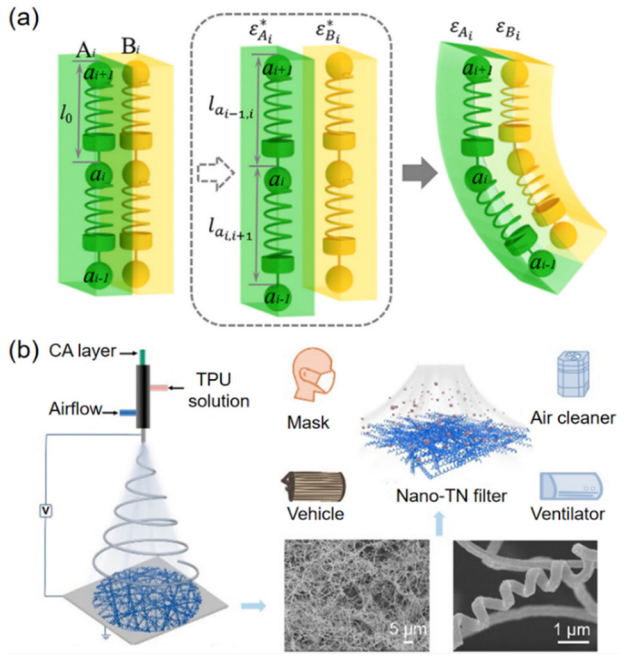

Fig. 4 Helical fibers are prepared by spinning. (a) The morphological development of helical structures in melt blown and electrospun fibers was simulated by calculating the intrinsic curvature within two-component fibers; reproduced with permission,[53] © 2020 Elsevier Ltd. All rights reserved. (b) Schematic diagram of the electroblown spinning process. Reproduced with permission,[54] Copyright © 2024, American Chemical Society.

side-by-side bi-group fibers with special self-bending, helical morphology and good mechanical properties are produced.[54] Since only PP with different MFRs is applied, this fiber will hopefully replace existing elastic fibers and be easier to recycle.[52] This work provides a scalable, convenient recycling method for the production of side-by-side two-component fibers with high curl rates.[53]

Wet spinning is a solution spinning technique in which the spinning solution is extruded through tiny holes into a solidification bath consisting of an undesirable solvent of the polymer. Once the spinning solution encounters a coagulant, it solidifies and precipitates into solid fibers. After stretching, shaping, washing, drying and other post-treatment processes, the helical fiber is finally obtained.

Melt-blown spinning is the use of high-temperature jet gas to rapidly stretch the polymer melt to obtain micro and nano fibers. The polymer is formed by the screw at high temperature and high pressure to form a thin stream of melt, which is extruded from the die spinnerets after passing through the corresponding distribution system. The high-temperature and high-speed draft air flow is blown out from both sides of the spinneret, so that the polymer melt thin stream is rapidly stretched and thinned. The microfibers formed by cooling and curing are evenly collected on the web curtain of the receiving device.

2.4. Liquid rope effect

Helical fibers can also be prepared by other methods, and the formation of helical fibers in microfluidic channels is based on

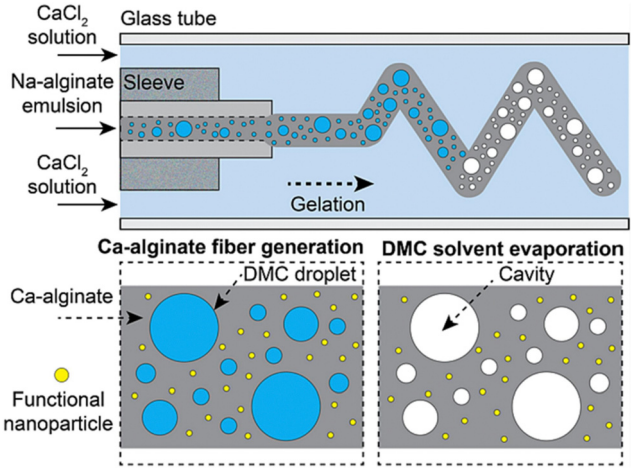

Fig. 5 Schematic diagram of a microfluidic process to generate microporous spiral hydrogel microfibers loaded with functional nanoparticles of calcium alginate (Ca alginate). Reproduced with permission,[56] © 2023 Elsevier Ltd. All rights reserved.

the phenomenon known as the "liquid rope-coil effect", which means that the viscous liquid flow tends to twist when it hits the surface under gravity, eventually forming a stable coil-like pattern.[55] The curing on polymers can be mainly divided into physical curing processes (such as solvent exchange, non-solvent-induced phase separation, solvent evaporation) and chemical curing processes (such as chemical cross-linking reactions, ion crosslinking reactions, photopolymerization reactions). As shown in Fig. 5, the solidification of calcium ions and sodium alginate resulting from a calcification reaction leads to the production of helical fibers. Microfluidic technology has a mature microfluidic product with high R&D cost, long cycle and great difficulty, and its development work includes chip design and processing technology, surface treatment process, supporting equipment design and assembly process, contained reagent development, system performance verification and other R&D work.[56]

2.5. Catalytic cracking

Helical carbon nanofibers with symmetrical growth patterns were synthesized by the decomposition of acetylene by a copper catalyst. There are always only two helical fibers that grow symmetrically on a single copper nanocrystal. The irregular tips and spiral inversions of the two helical fibers further reveal a symmetrical growth pattern. This mirror-symmetric growth pattern is caused by the shape change of copper nanocrystals during catalytic acetylene decomposition. Upon contact with an initial copper nanocrystal with an irregular shape, acetylene begins to break down to form two straight fibers (irregular tips). At the same time, the shape of the copper nanocrystals begins to change. As soon as they change from an irregular faceted shape to a regular faceted shape, the two straight fibers stop growing and the two regular spiral nanofibers with opposite spiral sensations begin to grow. If the regular faceted nanocrystals continue to change shape during fiber growth, both helical fibers may change the spiral sensation at the same time,

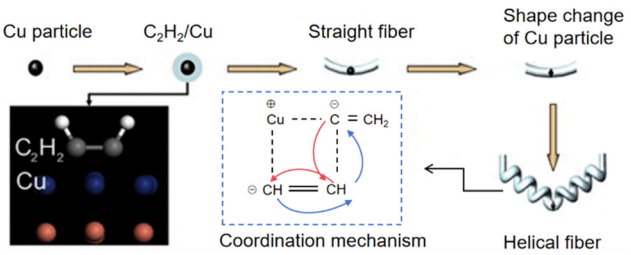

Fig. 6 Growth mechanism of coordination polymerization and asymmetric growth between acetylene and Cu surfaces. Reproduced with permission,[58] Copyright © 2010 Elsevier Ltd. All rights reserved.

resulting in helical inversion. The shape change is caused by a change in the surface energy of acetylene adsorbed on copper nanocrystals.[57] Fig. 6 illustrates the growth mechanism of coordinated polymerization and asymmetric growth of copper and acetylene in a unique crystal plane to explain the structural and morphological changes of nanofibers.[58]

2.6. Helical structure composed of asymmetrical forces

In general, the helical assembly of synthetic molecules can be initiated by introducing chiral elements such as chiral centers or chiral axes into the building molecule, where the chirality of the molecule can be expressed in the form of a helix. Interestingly, in some cases, achiral molecules can also form helical assembly upon adding an asymmetrical force to the system.[59] It is generally well established that formation of supramolecular aggregates occurs through a bottom-up process, involving cooperative intermolecular forces such as π–π stacking and hydrogen bonding, combined with other weaker and nondirectional interactions, very often leading to fibers possessing complex superstructures. Moreover, it has been emphasized that the presence of chiral alkyl chains at the periphery of the molecule which engage in the self-assembly process can trigger the preferential formation of only one helicity, as an expression of hierarchical organization at different levels.[60] In this regard, Palmans *et al.* introduced a very interesting building block with C_3 symmetry, consisting of a central aromatic ring functionalized at positions 1, 3 and 5, with a substituted *N*-monoacylated 3,3′-diamino-2,2′-bipyridine unit (Fig. 7).[61] Due to steric hindrance around the central aromatic core, the three bipyridine wedges that are self-rigid due to intramolecular hydrogen bonding adopt a propeller-like conformation, and in addition, the π–π stacking interaction results in the establishment of a columnar stack with a helical supramolecular structure.

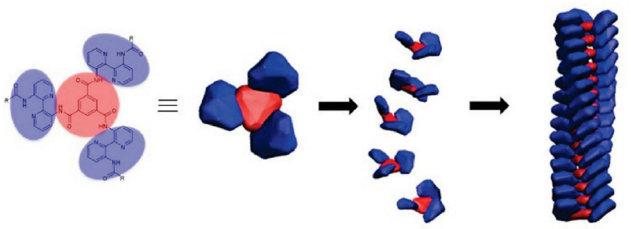

Fig. 7 Schematic model of the self-assembly of twisted stacks of C_3 symmetric *N*,*N*′,*N*″-tris[3(3′-carbamoylamino)-2,2′-bipyridyl]-benzene-1,3,5-tricarbonamide derivatives. Reproduced with permission,[60] Copyright © 2011, American Chemical Society.

3. Preparation method of helical fibers

Helical fibers are prepared in a variety of ways. At present, there are many methods for preparing helical fibers, mainly including the template synthesis method,[62] laser direct writing technology,[63] vapor phase chemical deposition (CAD),[64] wet spinning,[65] melt/dry spinning,[52,66] electrospinning and microfluidic spinning.[67,68]

3.1. Mechanical twisting

Mechanical twisting refers to the process of fixing one end of a fiber or film and applying an external force to the other end to rotate and wind around its own axis. As the degree of twisting gradually increases, eventually a helical structure of fibers is formed. The specific operation is as follows: first, fibers with spiral structure can be obtained by mechanically twisting the parallel primary fibers, and a micron-sized gap is formed between adjacent primary fibers. Then, during further twisting, many coils gradually form when the angle of rotation exceeds a certain critical point. Finally, after the formation of a tight longitudinal coil, a high-density fiber bundle is gradually formed, with a large gap between adjacent spiral coils. Spiral scaffolds are manufactured by continuously twisting the arranged nanofibers into yarns and then excessively twisting them into a spiral yarn. This spiral scaffold has special stretchability and toughness; it can be stretched up to 15 times its initial length. What's more, this layered material as a fiber scaffold undergoes non-affine deformation, and the stretching degree of seed cells is significantly less than that of the entire scaffold, simulating the natural curly fiber tissue.

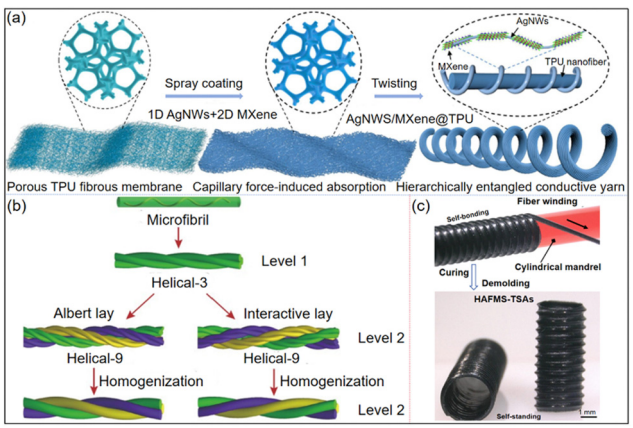

Fig. 8 (a) Structural evolution of layered interlocking spiral conductive yarns. Reproduced with permission,[69] © 2023 Elsevier B.V. All rights reserved; (b) schematic diagram of chiral assembly of fibrils from primary to secondary and the corresponding homogenization treatment. Reproduced with permission,[70] Copyright © 2023, The Chinese Society of Theoretical and Applied Mechanics and Springer-Verlag GmbH Germany, part of Springer Nature; (c) flexible bending HAFMS-TSA. Reproduced with permission,[71] Copyright © 2023 The Authors, some rights reserved; exclusive licensee American Association for the Advancement of Science.

Achieving high mechanical elasticity and electrical conductivity at the same time is a basic requirement for wearable electronics and smart fabrics. However, due to the "trade-off" effect between them, there are still significant challenges in achieving high conductivity under large mechanical deformations. Inspired by the curly structure of climbing plants, Zhang *et al.* developed a layered interlocking spiral conductive yarn for superstretched electronic and smart fabrics through a multi-dimensional synergistic conductive network of super-twisted silver nanowires (AgNWs)/MXene entangled with an elastic thermoplastic polyurethane (TPU) nanofiber network,[69] as shown in Fig. 8a. High-aspect-ratio 1D AgNWs bridge 2D MXene nanosheets into a synergistically interconnected conductive network while interlocking with an elastic 3D TPU nanofiber backbone. Based on the layered chiral structure of biofibers, a typical self-similar helical assembly process is shown in Fig. 8b.[70] In the case of Albert laying, the twisting direction or rotationality of the two stages of the fibers remains the same, while in the case of cross-laying, the fibers exhibit different winding rotationality. The number of fibrils may vary at different levels. As shown in Fig. 8b, a strand consisting of three fibrils in the second layer can be homogenized into a chiral rod. With similar helical assembly, the fibrils at layer 3 and higher can be further assembled.

In addition, Hu *et al.* developed a programmable filament winding platform for bottom-up construction of helical-artificial fibrous muscle structured tubular soft actuators (HAFMS-TSAs) that exhibit diverse tunable morphing behaviors embedded in their bioinspired 3D helical fiber architectures.[71] As shown in Fig. 8c, the filament is wound around a tubular die to obtain a flexibly bent HAFMS-TSA.

Mechanical spinning is a traditional spinning method that mainly uses mechanical equipment to draw raw materials such as coarse cotton, wool or silk into filaments. This method is fast and suitable for large-scale production. However, it has a higher cost and requires a lot of machinery and human resources.

3.2. Spinning technology

3.2.1. Wet spinning. The advantage of wet spinning is that it is easier to control the process in the first place: because the liquid encapsulates the particles well, the wet process allows for more precise control of the various parameters of the process, such as temperature, concentration, acidity, alkalinity, *etc.* The material can then be better protected: for some materials that are susceptible to oxidation or other contaminants, the wet process can better protect them, allowing them to remain stable for a long time. Secondly, it can also be applied to a variety of different material processing, such as metal, non-metal, ceramic, glass, *etc.* In addition, the wet process can produce a fine product with high purity and quality. Besides, the wet spinning process can also be combined with other processes to produce helical fibers, which are described in detail in the following sections. Wang *et al.* reported a multifunctional conductive helical fiber through a wet spinning and winding process.[50] The spiral-gel-based fiber matrix (sodium alginate (SA)/polyacrylic acid (PAA)) and the surface-deposited bilayer conductive layer ($Ti_3C_2T_x$ (MXene)/poly(3,4-ethyldioxythiophene) (PEDOT)) together form the necessary core–shell structure. Spiral SA/PAA hydrogel fibers (SP HF) were prepared by traditional wet spinning. The precursor solution consisting of SA and PAA was extruded directly into a coagulation bath solution containing 0.5 wt% $CaCl_2$ using flat-headed syringe needles. The helical structure was further prepared by secondary ion crosslinking. The initial hydrogel fibers collected from the coagulation bath are wound on Teflon rods and then immersed in $FeCl_3$ aqueous solution (Fig. 9). Different helical fiber templates can be obtained by adjusting the diameter of the control lever and the spacing of the windings.

Wet spinning is characterized by a complex technological process, large investment, low spinning speed and high production cost. Generally, in the production of staple fibers, multi-hole spinnerets or graded spinnerets can be used to increase production capacity, so as to compensate for the defect of low spinning speed.

3.2.2. Electrospinning. Electrospinning is a very versatile technique to produce continuous fibers, and electrospun fibers have found broad applications in air filtration,[72–75] actuation,[76,77] wastewater treatment,[78–81] electromagnetic shielding,[82–84] and so on. Especially electrospinning can also be successfully applied for the production of helical fibers by different methods.[85] Composite electrospinning appeared through the improvement of the nozzle

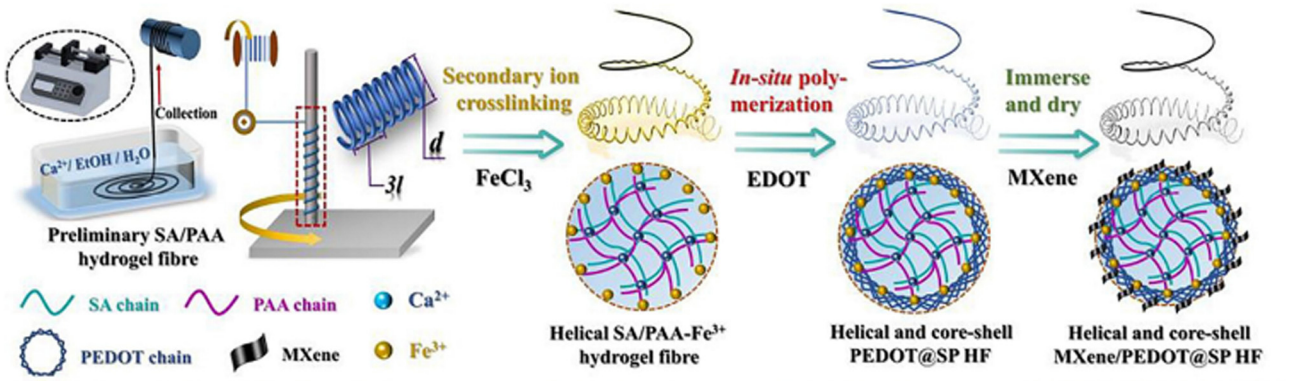

Fig. 9 Schematic diagram of the design and manufacture of conductivity stabilization and integrated MXene/PEDOT@SA/PAA fibers with helical and core–shell structures. Reproduced with permission,[50] © 2022 Elsevier B.V. All rights reserved.

structure. According to the structure of the nozzle used, composite electrospinning can be divided into the following types: shoulder-to-shoulder electrospinning, coaxial electrospinning and eccentric electrospinning.[49]

Du *et al.* applied PEO as the core component and PHB as the shell component. The PEO/PHB core–shell microfibers with spiral structure were prepared by coaxial electrospinning technology, a method for electrospinning side-by-side two-component polymer nanofibers using a microfluidic device as a spinning instrument.[86] Additionally, in Section 2, we have reported that the difference of shrinkage between different polymers is one of the factors that lead to the formation of helical fibers. Lin *et al.* reported that a kind of self-crimping nanofibers were prepared by using elastic polymer polyurethane (PU) and thermoplastic polyacrylonitrile (PAN) as raw materials.[8] Based on the same principle, Li *et al.* demonstrated a dual-spinneret electrospinning method that can directly generate three-dimensional self-crimping fibers. In this process, two spinnerets are used to prevent the solution from forming a gel or polymer precipitate. And the voltages of opposite polarity are applied to the spinneret separately, as shown in Fig. 10a. Li *et al.* selected two polymer components, TPU and cellulose acetate (CA), with different mechanical properties, to process into helical fibers.[87] Fig. 10b shows an image of a helical fiber nonwoven sample, which was prepared at 12 wt% TPU and 14 wt% CA.

Three-fluid electrospinning is a new improvement on traditional electrospinning. With this technique, three different polymer fluids can be electro-spun into a micro/nanofiber designed with a three-layer morphology. A novel type of multilayer nanofiber with helical and slot/hollow structures was prepared. Based on the fiber formation mechanism, cellulose acetate is combined with other appropriate polymers to generate spiral groove/hollow nanofibers using the designed three-fluid electrospinning system. By changing the capillary structure of the spinneret, fibers with spiral grooves and spiral hollow structures are obtained. Fig. 11a illustrates the preparation principle of multi-level nanofibers.[88] That is, in three-fluid electrospinning, using appropriate polymers and spinneret structures, a novel multi-level structure nanofiber with spiral groove/hollow structure was designed and successfully prepared. Due to the asymmetrical arrangement of the polymers of different components in this structure, the resulting fibers produce different shrinkage deformation after corresponding treatment, resulting in spiral curling. Helical fibers can be formed with parallel structures. Gai *et al.* used only one polymer of polypropylene (PP) with two different melt flow rates (MFR) as two components, and by adjusting the processing conditions, they produced side-by-side double-group fibers with special self-curvature, spiral morphology and good mechanical properties (Fig. 11b).[54] Since only PP with different MFRs is applied, this fiber has great promise to replace existing elastic fibers and is easier to recycle. Compared to the above methods, the most commonly used method is electrospinning technology. Electrospinning offers the following advantages. The fiber diameter is adjustable: this technology can adjust the diameter of the fiber over a wide range, from hundreds of nanometers to tens of microns, and even smaller. This adjustability is important because certain properties of a fiber (*e.g.*, water absorption, electrical conductivity) are closely related to its diameter, and adjusting the diameter allows the resulting fibers to be used in a variety of applications. Diverse fiber forms: electrospinning

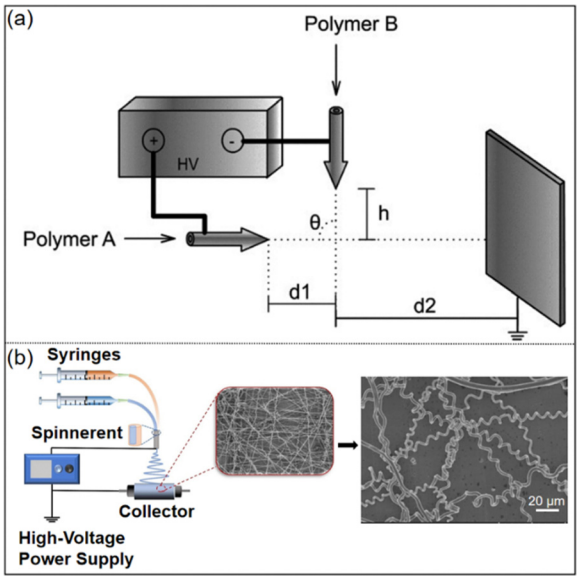

Fig. 10 Schematic diagram of the eustatic spinning system. (a) Double-spinneret electrospinning device for generating self-crimping composite polymer fibers. Reproduced with permission,[49] Copyright © 2011 Wiley Periodicals, Inc; (b) schematic diagram of TPU/CA helical fiber nonwovens and raw SEM images of the sample. Reproduced with permission,[87] Copyright © 2024, The Author(s), under exclusive licence to the Korean Fiber Society.

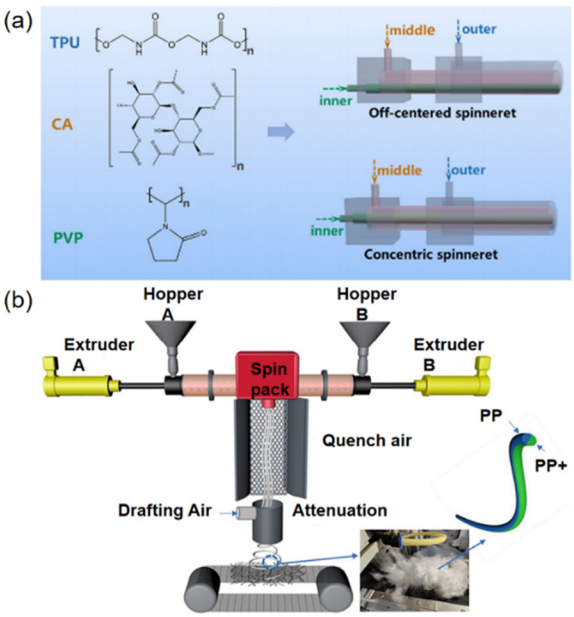

Fig. 11 (a) Principles of preparation of nanofibers with multi-level structures. Reproduced with permission,[88] Copyright © 2021, Elsevier; (b) side-by-side two-component spinning schematic. Reproduced with permission,[54] © 2023 Elsevier B.V. All rights reserved.

technology can produce a variety of different forms of fibers, including straight lines, spirals, loops, and more. These forms of fibers can be used according to different applications and can be easily switched during spinning. Strong adaptability to fiber materials: electrospinning technology is adaptable to a variety of fiber materials. It can handle many different types of polymers, natural fibers, and inorganic materials, and the right material can be selected for spinning according to the needs of the application.

In a word, compared to other advanced textile technologies, electrospinning technology is relatively simple in terms of equipment and operation, and the preparation process is easy to control. Electrospinning technology allows the preparation of very fine fibers, the diameter of which can be adjusted from a few nanometres to tens of microns. These microfibers have a very large surface area and are able to improve the adsorption, catalysis and transport properties of the material. Electrospinning technology can use a variety of polymers and fiber precursors to prepare fiber materials, so that a variety of materials can be prepared, including nanofibers, composite fibers, hybrid fibers, *etc.*

3.2.3. Melt blown spinning. The diameter of the micro–nanofibers prepared by melt-blown spinning is generally 3–5 μm, and the finest time can reach the nanoscale. Therefore, its product structure is fluffy, the specific surface area is large, the air permeability is good, the porosity is high and the filtration performance is excellent. Non-woven fabrics with porous structure and good mechanical properties can be widely used in tissue engineering. In order to obtain excellent performance, Feng prepared polylactic acid (PLA) melt blown disordered mats (MBNDM) with different mold-to-collector distances (DCD), and Fig. 12a shows the preparation process of PLA MBNDM.[51] Hui Li *et al.* reported the preparation of spiral microfibers from polymer blends using melt blowing techniques.[89] Using elastomers and hard polymers as raw materials, microfiber nonwovens are prepared by a designed rotary fusion blowing device. In this work, the influence of various parameters on the formation of helical fibers is discussed, such as the interfacial interaction between the polymer structure and the polymer components, the air-flow field characteristics and the processing parameters. The melt-blown device and its cross-sectional diagram are shown in Fig. 12b.

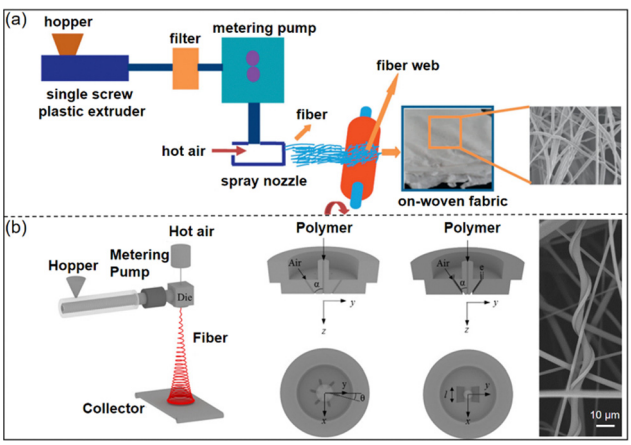

Fig. 12 (a) Schematic of the melt blown device used to prepare poly(lactic acid) (PLA) melt blown non-woven disordered mats (MBNDM). Reproduced with permission,[51] © 2016 Elsevier B.V. All rights reserved. (b) Schematic diagram of the melt blowing device, swirl die cross-section and end view, groove die section and end view. Reproduced with permission,[89] © 2018 Wiley Periodicals, Inc.

Melt-blow molding (MB) is a one-step process for the production of microfiber nonwoven materials in which the molten polymer is dispensed through a mold with a capillary tube, typically with a micron diameter, into a jet of high-speed subsonic hot air. The air jet accelerates the flow of the polymer, causing it to deform and vibrate violently. The expansion of a high-velocity air jet from the tank lowers the air temperature, which cools the molten polymer. Subsequently, the polymer gradually solidifies and deposits on the moving current collector, forming bonds between the fibers and creating a non-woven web.[90] Melt blown nonwovens can be used for filtration, sound insulation, medical and health care, battery separators, oil absorption, and warmth preservation due to their fluffy structure, good air permeability, and high porosity. The main characteristics of the melt blown spinning method are high winding speed, no need for solvents and precipitants, simple equipment, short process flow, and an economical, convenient and efficient method. However, the number of spinneret holes is relatively small.

3.2.4. Helical fibers by combining different methods. In addition to a single method for preparing helical fibers, there are many researchers who combine multiple methods to produce helical structures. For instance Zhao *et al.* reported a high-performance SFSC of dry-spun fibers with a double helix-wound structure impregnated using ultra-thin gold nanowires (AuNWs).[91] Guided by Hildebrand and Hansen solubility parameters, small amounts of AuNWs were well dispersed in tetrahydrofuran (THF) solutions of styrene-ethylene/butylene-styrene (SEBS) polymers to form highly stretchable fibers in a stretchable dry spinning process. During the spinning process, a strand of spinning liquid is extruded from the needle and dried directly in the air at room temperature to form elastic AuNWs/SEBS fibers. With the help of AuNWs partially exposed on the surface of the dry-spun fibers, a uniform gold film (AuFilm) is grown on the fibers through an electroless plating process to form a stretchable fiber conductor. The bonding between AuNWs and AuFilm ensures the interface structure of the fiber conductor over a wide strain range. AuNWs/AuFilm/polyaniline (PANI) hybrid fiber electrodes were constructed by the electrodeposition method using fiber conductors. The two electrodes are wound in parallel along the rubber core, and the gel electrolyte is coated to retain most of the capacitance under high strain. The fabrication process of the stretchable electrodes of this SFSC is illustrated in Fig. 13a–c.

Using the phenomenon of liquid rope coiling,[92] as shown in Fig. 14a, poly(ether sulfone) spiral hollow fiber membranes were obtained by dry and wet spinning.[93] By changing the coagulation value, PEG400 is added as a pore agent to change the composition of the polymer solution.[94] Liquid composition, coagulation bath temperature, air gap, polymer coating, and

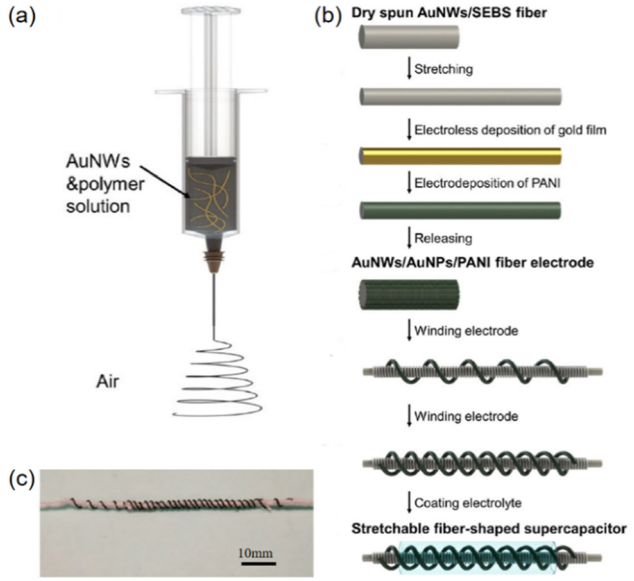

Fig. 13 (a) Schematic diagram of the dry spinning process; (b) schematic diagram of fabrication of stretchable AuNWs/AuFilm/PANI fiber electrodes; (c) photograph of two fiber optic electrodes wound in parallel in a double helical structure. Reproduced with permission,[91] Copyright © 2018, American Chemical Society.

liquid flow were varied to map the conditions for helical fiber formation. It has been observed that the increase in the air gap changes the geometry of the fibers from straight to spiral (Fig. 14b). Under the same spinning conditions, increasing the coagulation bath temperature causes the spiral geometry to become irregular or straight, probably due to the higher water vapor absorption in the air gap.

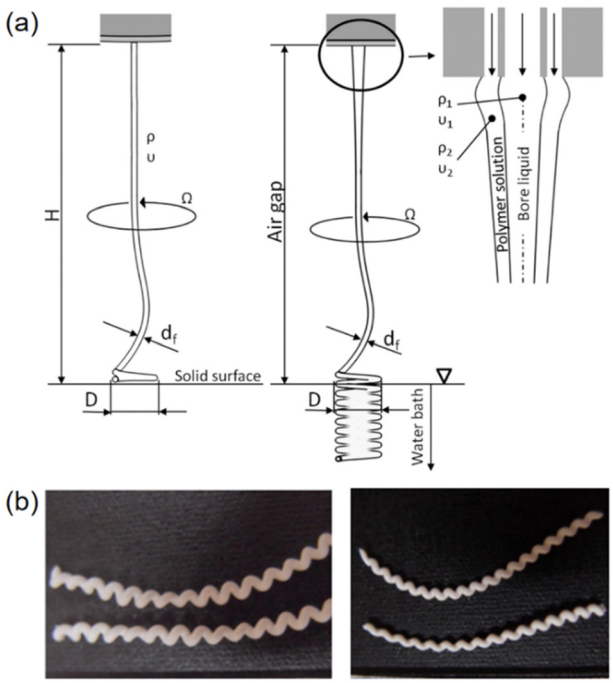

Fig. 14 (a) Schematic diagram of the rope coiling device. Reproduced with permission,[94] Copyright © 2024 The Royal Society; (b) photograph of a hollow fibrous membrane taken with an optical microscope. Reproduced with permission,[93] © 2018 Elsevier B.V. All rights reserved.

3.3. Sol–gel method

In recent years, there has been an increasing interest in low-molecular-weight compounds that can efficiently gelatinize various organic solvents when forming a network of fibrous aggregates. Kazunori *et al.* found that the fibers of certain ''cationic'' cholesterol derivatives gel a tetraethoxysilane (TEOS) solution and are efficiently transcribed to give a novel mesoporous silica with a tubular macaroni powdery structure.[95] The condensation of anionic silica preferentially occurs on the surface of the cationic aggregates. Under certain limited conditions, a unique right-handed ''spiral'' silica is obtained. Two possible reasons to explain the formation of the double helical structure are that TEOS polycondensation can be preferentially carried out along the groove-shaped plane of the twisted band with a high positive charge density. Alternatively, it can be preferentially carried out along the edge of the band, where the positive charge is less dense but more exposed to solvents. However, when condensation occurs on the surface, the distance between the fibrils is expected to be of the order of the band thickness, and when condensation occurs on the edge, the distance between the fibrils should be of the order of the bandwidth. The sol–gel transition of this system and the success of a novel double-helix silica fiber with adjustable spacing were confirmed.

3.4. Template method

Although there are many ways to obtain helical fibers, the template method is one of the most effective methods in order to obtain the specified morphology and predetermined microstructure. Here, W. J. Kim *et al.* present a very clear, new method for preparing flow-induced microstructures of inorganic spiral tubular mesopores by inducing so-called Taylor vortices.[96] Taylor vortices (or coil spring flows) can be created or completely eliminated in this flow unit simply by controlling the rotation speed of the inner cylinder. This cannot be achieved with traditional stirring. They prepared well-aligned mesoporous spiral silicon tubes from flow-cosurfactant templates. Its basic idea is very clear and elegant, and utilizes the flow-induced microstructure of insect-like cetyltrimethylammonium bromide (CTAB) micelles. Insectoid micelles form a well-defined helical structure under the flow of coil springs produced by Taylor's instability, and they maintain this structure under flow. The helical carbon fiber (HCF) is a new type of carbon fiber material, which has attracted much attention due to its distinctive characteristics, diversified novel properties and applications. However, the application of HCFs still faces a series of obstacles, especially in the repeated preparation of HCFs. Wang *et al.* preliminarily reported the synthesis of HCFs with ultra-high specific surface area using high-purity spiral containers (SVs) as templates through a biotemplate process.[12] The helical structure with ultra-high specific surface area can effectively shorten the route of antibiotic diffusion, and the high content of nanopores (1 to 3 nm) not only ensures the

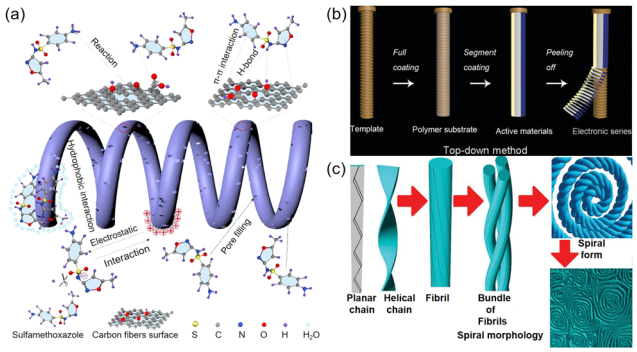

Fig. 15 (a) The porous spiral carbon fiber was prepared by a biomimetic process. Reproduced with permission,[12] © 2020 Elsevier Inc. All rights reserved; (b) the novel "top-down" method to obtain helical inorganic electronic devices that are highly stretchable, breathable and wearable based on the template of a simple screw. Reproduced with permission,[97] © 2024 Copyright Clearance Center, Inc. All rights reserved; (c) schematic diagram of a hierarchical helical structure from primary PA chains to helix morphology. Reproduced with permission,[98] Copyright © 2009, American Chemical Society.

accessibility of the antibiotic storage surface, but also easily provides a convenient passage for antibiotic transmission (Fig. 15a). In addition, Xu *et al.* proposed a novel and simple method for the preparation of helical fibers, which can convert a rigid device into a stretchable helical device by stripping the thermoelectric material from the screw,[97] as shown in Fig. 15b.

In addition to the one-dimensionally oriented polyacetylene (PA) fibril structure, spiral PA fibers are also synthesized in cholesteric liquid crystal (CLC) as a template for PA polymerization, and the template CLC contains chiral dopants with axial chirality (Fig. 15c).[64] When CLC with helical structure was used as the template for PA polymerization, PA fibrils with similar helical morphology could be obtained.[98]

The template method is considered to be an important method for active layer microfabrication of flexible tactile sensors.[99] It uses physical/chemical processes to introduce micro–nano structures on the active layer, resulting in improved performance such as sensitivity, response/recovery time, and detection limit. Therefore, the template method occupies a dominant position in micro–nano fabrication by virtue of its high precision and high reliability, which has attracted the interest of many researchers and made the rapid development of various templates.

3.5. Microfluidic technology

Microfluidic spinning technology is a typical wet spinning process. Compared to other spinning methods, microfluidic spinning technology combines microfluidic technology with chemical reactions, utilizing microfluidic chips to achieve precise fluid control. The inner phase solution takes advantage of its laminar flow properties to flow in the microchannel of the microfluidic chip in the direction of liquid flow without touching the inner wall of the microchannel. It undergoes a physical or chemical transformation to produce solid fibers within a microchannel or after spraying.[100]

As mentioned above, Liu *et al.*'s microfluidic technology is now widely used in the preparation of helical fibers.[55] Calcium ions are continuously delivered to the seaweed and the acid liquid is rapidly crosslinked on their contact surface, forming a high-viscosity alginate gel interlayer. Calcium alginate hydrogel has been widely used in microfluidic spinning because it is biocompatible and biodegradable. Alginate is a polysaccharide, which is a linear copolymer with guluronic (G-block) and epimer mannuronic (M-block) residues; alginate polymers containing G block undergo ionotropic gelation with Ca ions. Fig. 16a illustrates the principle of helical fiber formation *via* microfluidic technology. Spinning occurred first when the inner Na-alginate liquid flow was injected into a $CaCl_2$ solution, which formed a semigelation microfiber at the orifice of an injection capillary. This microfiber was then spiraled and solidified based on an unbalanced fluidic friction between the microfiber and its surrounding fluid,[6] as shown in Fig. 16b and c. Rotation occurs first when the internal sodium alginate liquid stream is injected into the calcium chloride solution, which forms semi-glue microfibers at the pores of the injection capillaries. This ultrafine fiber is then spiraled and solidified based on the unbalanced fluid friction between the ultra-microfiber and its surrounding fluid. Since these processes can be precisely adjusted by adjusting the flow rate, the length, diameter and pitch of the spiral microfibers are highly controllable. In addition, as a benefit of the rapid gelation process, the

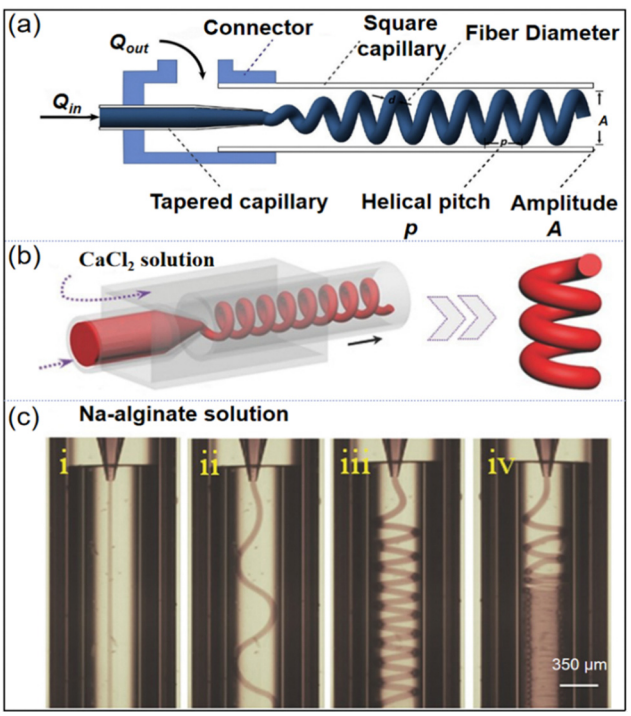

Fig. 16 (a) Preparation of microfibers based on the liquid rope coil effect, curling phenomenon on a longitudinal section of a coaxial device. Reproduced with permission,[55] © 2019 Elsevier B.V. All rights reserved; (b) and (c) Schematic diagram of the formation of spiral microfibers by microfluidics and four flow patterns at different flow velocities: (i) straight line, (ii) wavy, (iii) helix, and (iv) blockage. Reproduced with permission,[6] © 2017 WILEY-VCH Verlag GmbH & Co. KGaA, Weinheim.

synthesized helical microfibers maintain the same cross-sectional structure as the injection stream and are therefore endowed with structures such as Janus, triplet, core–shell, and even double helix.

However, it is difficult to achieve large-scale production of helical fibers prepared by microfluidic technology, and it is difficult to solve the quality control problems. But its advantage is that the consumption of samples and reagents is small, the cost is reduced, the reagents consumed for sample analysis are only a few microliters to tens of microliters, and the volume of the analyzed substance required is only nanoliters or picolitres (usually one hundredth or even one ten-thousandth or less), so that high-precision and high-sensitivity separation and detection is possible by using very few samples and reagents, reducing detection costs and shortening analysis time. With the characteristics of high throughput, fast analysis and detection speed, microfluidics can be designed as a multi-channel system; through the microfluidic channel network, the sample to be detected can be shunted to multiple reaction units at the same time, and since the reaction units are isolated from each other, each reaction does not interfere with each other and multiple items can be detected as needed with less pollution and small detection error.

3.6. Chemical vapor deposition

CVD is the main method for preparing helical carbon fiber, and has the advantages of good repeatability, high quality, considerable yield and easy control of experimental conditions, and is the most promising method for large-scale production of helical carbon fiber. Firstly, Motojima *et al.* successfully synthesized spiral carbon fibers by chemical vapor deposition using nickel powder as a catalytic particle, and the reproducibility was good.[101] Since then, more and more researches are focused on the structural design of spiral carbon fibers.

Carbon nanotubes (CNTs) are one of the most promising candidates for electromagnetic wave absorption due to their typical one-dimensional hollow structure, low seepage threshold, high aspect ratio, low density, adjustable diameter, and high dielectric loss.[102] The high temperatures required for CNT growth disrupt the MXene structure and oxidize it to TiO_2. When the structural integrity of MXene is compromised, it can no longer maintain a regular two-dimensional layered structure, resulting in the deterioration of its dielectric properties. In this study, Yang *et al.* performed *in-situ* growth of carbon nanotubes on $Ti_3C_2T_x$MXene achieved by vacuum chemical vapor deposition (CVD) at ultra-low temperatures (minimum 450 °C).[103] The ultra-low temperature effectively prevents the structural damage and oxidation of MXene. Without the addition of any additional nitrogen source except N_2, the grown carbon nanotubes have a bamboo-like structure with which helical carbon nanofibers coexist. This complex structure further enhances the reflective, scattering, and dissipating capabilities of the CNT/MXene (Fig. 17a) hybrids towards electromagnetic waves (EMWs).

3.7. Self-assembling helical fibers

Self-assembled structures, such as helical nanostructures, are of great interest and significance due to their critical role in sensors, imaging, and therapeutics, and some materials can easily form

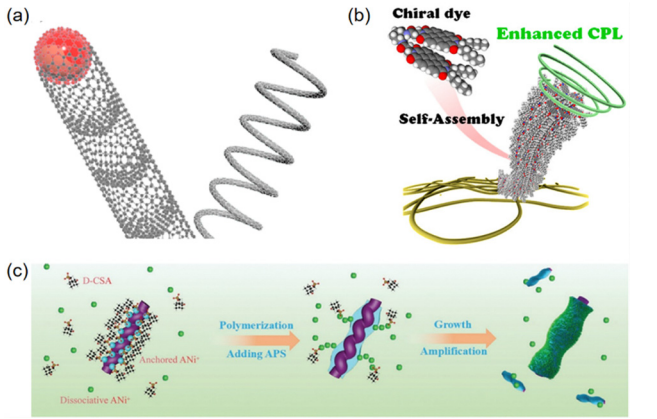

Fig. 17 (a) Demonstration of bamboo-like structure of CNT and spiral carbon nanofibers. Reproduced with permission,[103] © 2021 Elsevier Ltd and Techna Group S.r.l. All rights reserved; (b) schematic diagram of a chiral organic chromophore system and its self-assembly domain. Reproduced with permission,[104] © 2024 Copyright Clearance Center, Inc. All rights reserved; (c) schematic diagram of the preparation process and formation mechanism of CPANi@HPPy hybrid nanofibers. Reproduced with permission,[105] © 2023 Wiley-VCH GmbH.

self-assembled spirals.[106] Li *et al.* reported the preparation of helical light-emitting fibers with circular polarized luminescence (CPL) properties by self-assembly of chiral phenanthro[9,10-*d*]imidazole (PIM) derivatives.[104] They selected 1,2-diphenylphenol imidazole derivatives as scaffolds and modified them with D- and L-aniline to synthesize two chiral PIM molecules (PIM-D-Ala and PIM-L-Ala), respectively. The position of chiral motifs is key to control the chirality, self-assembly behavior, and optical properties of chiral PIM derivatives. Systematic studies have shown that the photoluminescence and electroluminescence of PIM derivatives are mainly due to the contribution of imidazole. The addition of chiral attachment introduces an asymmetric force field to the imidazole scaffold, inducing spiral rotation of the PIM scaffold, which can be stabilized by non-covalent interactions of chiral attachment, such as hydrogen bonding and van der Waals interactions (Fig. 17b). Then Li *et al.* found that chiral microwave absorption materials (MAMs) can generate additional magnetic losses without the addition of magnetic media due to their unique electromagnetic cross-polarization effect.[105] However, they also need to further improve the effective bandwidth of chiral MAMs and reveal the attenuation modes and modulation methods of chiral structures. Through the *in situ* polymerization strategy, a novel supercoiled nanostructure based on chiral polyaniline and helical polypyrene was successfully realized (Fig. 17c). In addition, Li *et al.* further explored molecular arrangement and interactions during assembly.[107] The driving force for helical fiber formation comes from the synergistic effects of intermolecular hydrogen bonding, π–π interactions, and spatial interactions, and further realizes the multi-scale chiral hybrid material with controllable structure through *in situ* absorption polymerization.

3.8. Other methods

In addition to the commonly used CVD method, other techniques can also be used to prepare spiral carbon fibers. Zhang

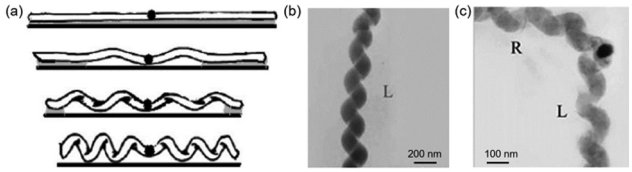

Fig. 18 (a) The growth mechanism of carbon coils is explained from top to bottom. Reproduced with permission,[108] Copyright © 2007 Elsevier Ltd. All rights reserved. The gray and dark areas represent van der Waals area and sheet metal, respectively; (b) left-handed helical structure and encapsulated catalytic particles; (c) right-handed helical structure and encapsulated catalytic particles. Reproduced with permission,[109] Copyright © 2008 Published by Elsevier B.V.

et al. synthesized carbon coils by decomposition of acetylene using the arc discharge method under different gas pressures from 160 to 460 Torr over a metal plate.[108] The advantageous feature of their method is that there is no need for the complex preparation of the catalyst particles and the introduction of the impurities. Their experimental apparatus is composed of a spectral pure graphite rod as the anode, a metal plate as the cathode, acetylene as the carbon source, reaction chamber, vacuum pump, circulatory system, DC power supply, *etc.* At a voltage of 35–40 V and an output current of 96 A, an arc was generated in an acetylene atmosphere and at a pressure of 160–460 Torr. After three minutes, the club-shaped products of approximately 1 mm in size deposited vertically over the surfaces of the plate (Fig. 18a). Carbon nano coils (CNCs) were synthesized *in situ* in an ethanol flame using a tin oxide nanoparticle catalyst using tin chloride precursors.[109] The anisotropic deposition rate of carbon between the tin dioxide crystal planes provides the driving force for the winding of carbon fibers. The resulting CNCs have tight coil spacing, with average fiber and coil diameters of about 50–80 nm and 80–100 nm, respectively. BET measurements and the Barrett–Joyner–Halenda (BJH) method show that CNC CPUs have mesoporous properties. CNC CPUs have excellent specific capacitance. The electrode with a polarization of 40 F g^{-1}, which is significantly higher than that of micro-helical carbon fiber or carbon nanofiber, may be ideal as a supercapacitor. The TEM image of a carbon coil on a tin oxide nanoparticle synthesized in an ethanol flame is shown in Fig. 18b and c.

Compared with the above-mentioned methods for preparing spiral carbon fibers, the chemical vapor deposition method is mostly used for the preparation of spiral carbon fibers, which has the advantages of low cost, large yield, and easy control of experimental conditions, and is the most promising method to achieve large-scale preparation of high-quality spiral carbon fibers. Chemical vapor deposition is a commonly used method of fiber preparation in which a chemical reaction occurs in the gas phase to create a fibrous structure on a substrate. The CVD method can prepare fibers of a variety of materials, such as carbon fiber, carbon helix fiber, *etc.* Characteristics such as composition, morphology, and size of fibers can also be controlled to meet a variety of needs. At the same time, it also offers a fast growth rate, uniform fiber structure, and stable and reliable quality. Therefore, the fibers prepared by the CVD method have excellent performance and structural characteristics, and are widely used in materials science, nanotechnology, electronics and other fields.

The biggest advantage of using co-condensation to prepare helical fibers is that the organic groups can be relatively uniformly distributed in the pores of the material, but because some of the functional groups introduced are dispersed in the pore walls of mesoporous molecular sieves, this affects the condensation between species to a certain extent, so that the crystallinity and order of molecular sieves are reduced. In particular, when the concentration of functional molecules is high and the volume is large, the impact is greater, so the number of organic groups introduced by the co-condensation method should be limited. For example molecular recognition properties are used in the preparation of molecularly imprinted hybrid silica. The matrix can be prepared by co-condensation of cyanurate (CA) with tetraethyl orthosilicate (TEOS) in the presence of non-silyl amines (used as templates). The latter is completely removed by washing the mixed material with hydrochloric acid. It can be reintroduced by mixing the resulting matrix with an aqueous suspension of melamine. These tapes were monitored and analyzed with various techniques: solid-state nuclear magnetic resonance (NMR) (29Si, 13C), Fourier transform infrared spectroscopy (FTIR), and nitrogen adsorption-adsorption measurements.[110] Hygroscopic spiral drives can also be utilized to prepare autonomous self-buried seed carriers for aerial sowing.[111]

From the above, it can be seen that the development of helical fibers is gradually increasing, and the methods of preparing helical fibers are also endless, and a single technology can be used to prepare fiber, or a combination of technologies can also be adopted to achieve excellent preparation performance and low-cost fiber. However, different methods can be used to obtain fibers with different properties; the different approaches for preparing helical fibers are summarized, and their advantages and disadvantages are compared in Table 1.

4. Properties of helical fibers

As a high-performance fiber, the helical fiber exhibits many excellent properties due to its unique molecular structure and morphology. This section will focus on the lightness and softness, good hydrophobicity, high electrical conductivity, and high stability and strength of helical fibers. These excellent characteristics make helical fibers have a wide range of application prospects in textile, medical, environmental protection and other fields.

4.1. Flexibility of helical fibers

A spiral or helix shape is usually made by wrapping a conductive wire/tape around a molded model that may act as a spring. The helical shape has a large stretch due to the presence of multiple spiral coils along the axial direction, which can disperse large deformations into small parts.[128] This structure can be well applied to materials with poor tensile properties (such as metal electrodes) to achieve good flexural properties

Table 1 Advantages and disadvantages of various methods for preparing helical fibers

Preparation method	Merit	Shortcoming	Ref.
Mechanical twisting	-Increases the twisting of the fibers -Increases the bendability of the fibers -Improves the processability of fibers	-It is not conducive to lightweight design -Increases brittleness	112
Wet spinning	-The fiber is of high quality -Special fibers can be produced	-The equipment is complex and costly -It requires the use of more chemicals	113
Electrospinning	-Simplicity -Cost effectiveness -Mass production is possible	-Sensitive to a lot of parameters -Evaporation rate control -Difficult to handle individual fibers	114
Melt blown spinning	-High production efficiency -The cost is lower	-Complex process -There are many influencing factors	115
Sol–gel method	-Can achieve uniform doping at the molecular level -The temperature is low -A variety of new materials can be prepared	-High cost and harmful to health -It takes a long time -A large number of micropores	116
Template method	-Light weight; good permeability -Large specific surface area -Strong adsorption capacity	-Poor mechanical properties -Difficult to prepare structurally adjustable fibers	117
Microfluidics	-A mild spinning environment -The fiber size and shape are uniform -The ability to handle single fiber	-It is expensive to manufacture -Difficult to control precisely -Difficult to operate	118
Chemical vapor deposition	-There are no sedimentary sight shadows -It has a high deposition rate -Good adhesion	-A closed system is required -The cost of reactants is high -Low use of reactants	119
Magnetically actuated helical fibers	-Strong magnetic response -Broad application prospects -Adjustable magnetic properties	-Reduced fiber strength -Complex spinning equipment -Risk of magnetic contamination	120
Heat-responsive helical fibers	-High temperature sensitivity -Programmability -Versatility	-Limited material selection -Complex preparation process -Stability issues	121
Ultraviolet-induced helical fibers	-Strong photosensitivity -UV protection function -Morphological controllability	-Preparation complexity and cost -Performance stability -Application limitations	122
Arc discharge method	-The equipment is simple; low cost -Raw materials are readily available	-The yield is not high -There are many defects	123
Flame method	-High precision and efficiency -Diversified and stable quality	-High energy consumption -Environmental pollution	124
Co-condensation method	-The process is simple -Reaction conditions eased	-A large amount of solvent -Slow reaction time -Not easy to refine	125
Dry spinning	-Low cost -Easy to operate	-The fiber quality is uneven -It is not possible to produce special functional fibers -Organic solvents are required	126
Hydrothermal method	-The reaction conditions are mild -Improves performance -Homogeneous and fine product	-Long reaction time -It is difficult to control the reaction conditions -High-precision reactors are required	127

and tensile properties.[129] Zamarayeva *et al.* designed an Ag–Zn cell with a flexible helical structure consisting of an electrogalvanized anode, a dip-coated polyvinyl alcohol (PVA) electrolyte, cellophane-wrapped on a prefabricated tinned copper spiral ribbon current collector, and a silver cathode.[130] The helical silver–zinc battery with a minimum bending diameter of 10 mm has an initial specific discharge capacity of 1.33 mA h cm^{-1}, with slight capacity fluctuations in the continuous operating state of bending deformation (Fig. 19a and b).

It is believed that the increase in the effective surface area of the silver electrode caused by bending deformation enhances the capacity of the flexible battery. Liu *et al.* designed a helical copper-based flexible lithium metal anode that can be stretched in a two-dimensional plane.[131] The capacitance of the stretchable lithium metal anode is about 1 mA h cm^{-2}, and there is no significant difference in the voltage curve (Fig. 19c–e) and cycling performance (Fig. 19f) between the unstretched and 60% tensile states, confirming the good tensile stability of the electrode. In general, spiral electrodes have spring-like properties that allow them to be highly stretched or bent, making them a good choice for increasing the flexibility of rigid electrode materials.

4.2. Hydrophobicity of helical fibers

Wearable electronic devices are in contact with human skin for a long time and exchange dynamic heat and humidity with the external environment. Therefore, in addition to having excellent electromechanical properties and high wear resistance, electric textiles are also required to have good comfort (breathability) and adaptability (waterproof). Zhang *et al.* reported that polyvinylidene fluoride-trifluoroethylene (P(VDF-TrFE)) materials continuously twisted into a unique Fermat helix nanostructure had good hydrophobic properties, and Fermat-spiral-based energy yarn (FSBEY) exhibited robustness and high hydrophobicity.[132] Fig. 20a shows the rapid rolling of water droplets on the surface of the FSBEY. The filament is highly hydrophobic in both the original and tensile states, with a

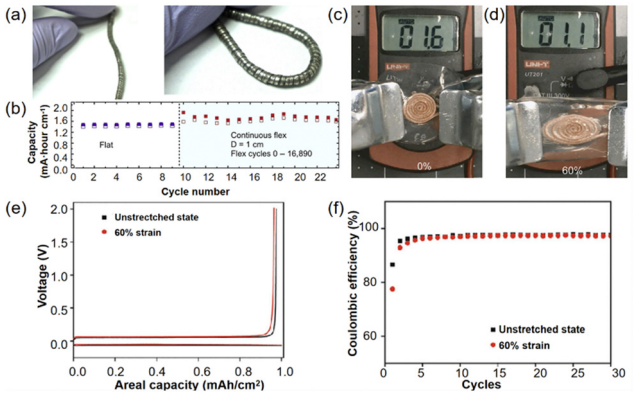

Fig. 19 (a) Photograph of a flex wire battery in a flat and bent state; (b) cyclic performance of a wire battery in a flat state and when bent to 1 cm curved diameter. Reproduced with permission,[131] © 2018 Published by Elsevier Inc. Output voltage of the helical stretchable battery: (c) flat and (d) 60% stretched; (e) voltage curves and (f) cycling performance of helical stretchable lithium metal anodes in unstretched and 60% stretched states. Reproduced with permission,[130] Copyright © 2017, The Authors.

contact angle of approximately 145°[133] (Fig. 20b). They designed a piece of FSBEY knitted e-textile (8 × 8 cm) using a hand-cranked flatbed machine. The interconnected yarn loops of e-textiles give them good air and moisture permeability. Water vapor and heat can be efficiently exchanged between the skin and the environment (Fig. 20c). At the same time, we quantitatively characterized the moisture permeability in FSBEY knitted e-textiles using a moisture management tester (MMT). The hydrophobicity of the droplets on the surface of FSBEY knitted e-textiles was further explained according to the Young–Laplace equation.[134] The droplet (1 wt% sodium chloride (NaCl) solution as simulated sweat) can maintain its shape on the top surface (hydrophobic layer) of the e-textile without being absorbed by the underside of the e-textile for at least 120 seconds, exhibiting excellent water repellency. Gao *et al.* prepared thermoplastic polyurethane (TPU)-based helical fibers, which are illustrated in Fig. 20d, that float on water and automatically repair overstretched displays under heat.[135] Deformation and damage of helical fibers can be recovered in 200 ms in water at 80 °C. Due to their hydrophobic nature and low density, they float on the surface all the time, which makes them of higher application value in the field related to surface sensing.

4.3. Electrical conductivity of helical fibers

The rapid development of wearable electronics is profoundly reshaping our daily lives. At the heart of these innovations, stretchable conductive optical fibers (SCFs) play a key role in highly sensitive strain sensing and highly conductive flexible conductivity. Stretchable conductive core sheathed fibers (SCCFs) with a three-dimensional helical structure are designed to be flexible and conductive with low resistance sensitivity under large strains. Yu *et al.* found that the relative resistance change of the spiral SCCF-strain curve fluctuates due to a change in the helical structure, accompanied by the elongation of the conductive path,[136] as shown in Fig. 21a, where the conductivity varies with the elongation of the SCCF. The conductivity of this helical SCCF remains stable as the strain and tensile rate increase, as shown in Fig. 21b. These evaluations of conductivity and reliability show that this spiral-shaped SCCF is capable of being a flexible conductor of electricity in wearable electronic devices.

However, conductivity is often influenced by tensile strain. Lu *et al.* prepared core–shell nanofiber helices, *i.e.*, LM@PU/SF helices, based on the super elasticity of polyurethane (PU), silk fibroin (SF), and liquid metal (LM), which exhibited good conductivity mainly due to the stable conductive pathways formed by the vertical and horizontal penetration of LM during the twisting process.[137] Due to the good fluidity of LM, the porous fiber network, and the restricted extrusion during twisting, the LM is prone to horizontal and vertical penetration throughout the entire fiber network (Fig. 21c). The resultant

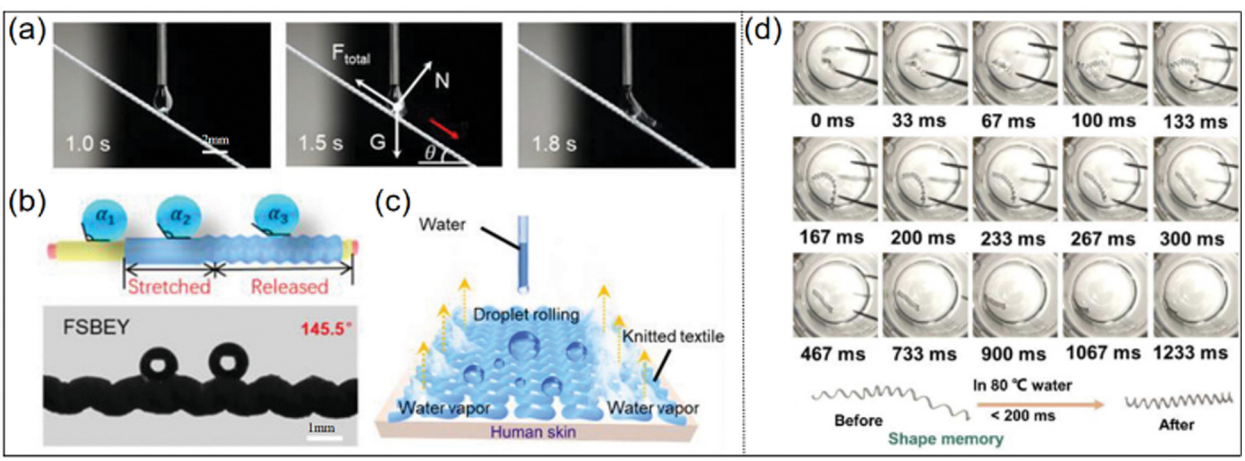

Fig. 20 Water resistance of FSBEY and its knitted e-textiles. (a) The process of water rolling down (flow rate 5 μL min^{-1}) on the inclined (35°) FSBEY (*N*, *G* and *F* are the total normal force, droplet gravity and drag, respectively); (b) water contact angle (WCA) between the yarn electrode and FSBEY ($\alpha_3 > \alpha_2 > \alpha_1$); (c) schematic diagram of the waterproof and breathable mechanism of FSBEY knitted electronic textiles. Reproduced with permission,[132] © 2021 Wiley-VCH GmbH. (d) Hydrophobicity and self-healing properties of TPU helical fibers. Reproduced with permission,[135] © 2024 Elsevier B.V. All rights reserved.

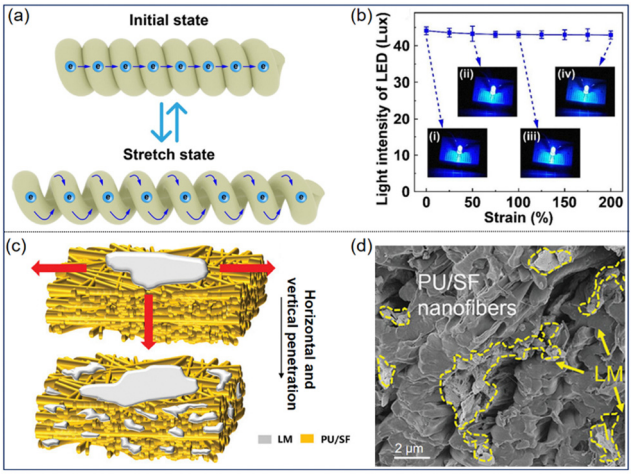

Fig. 21 (a) Illustration of the elongation of the conductive path of the helical SCCF which is stretched; (b) the light intensity of the spiral SCCF LED under different strain conditions shows high and stable conductivity. Reproduced with permission,[136] Copyright © 2024, Elsevier. Schematic diagram (c) and SEM image (d) of horizontal and vertical penetration of LM during stretching. Reproduced with permission,[137] © 2024 The Authors. Advanced Electronic Materials published by Wiley-VCH GmbH.

conductive paths on the surface and inside (Fig. 21d), allowed the composite fiber helix to remain conductive even when axially stretched.

4.4. Cyclic stability of helical fibers

Due to the unique spiral geometry, different functional helical fibers can be manufactured to perform important tasks, including cargo transportation, medical treatment, cell manipulation, and more. Although microfluidic technology is widely used in the fabrication of helical fibers, the problems of channel clogging and spinning instability have not been well solved, which limits the large-scale preparation and practical application of spiral microfibers. Ma *et al.* used an inner core stainless steel needle with a sleeve instead of a conical capillary, and in order to demonstrate the performance of the microfluidic device, sodium alginate solution and calcium chloride solution were selected as the internal and external phase fluids, respectively.[138] Spiral microfibers with different pitch values, wire diameters, and amplitudes were successfully fabricated in a uniform and controlled manner under the fine control of the flow velocity of the inner and outer phases, as shown in Fig. 22. In addition, the stability of the spiral morphology of the microfiber is also very remarkable. It can spin continuously for an hour without deformation and is rarely clogged. This reflects the long working life and robustness of our channel.

When the bacterial cellulose (BC) helical fiber prepared by Liang *et al.* was stretched for 100 cycles at 100% tensile elongation, the ring opening of the helical structure in the first cycle was relaxed, and the weak hydrogen bond between the nanofiber network and the inner matrix of the helical fiber was broken, resulting in a strain recovery rate of 88%.[139] It can be observed that the tensile recovery remains essentially constant over the subsequent 2–100 cycles due to helical geometry effects and reforming hydrogen bonding at the new position, indicating

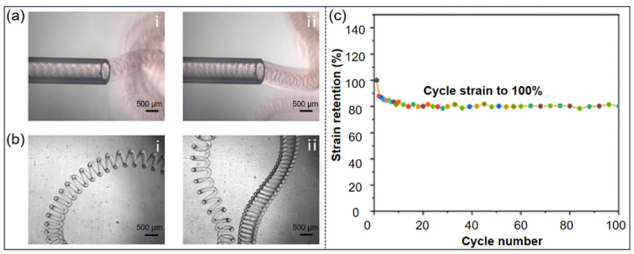

Fig. 22 Helical microfibers are fabricated by using an improved microfluidic device. (a) The different morphologies of the helical microfibrils observed at the outlet: (i) helical microfibrils with relatively large helix spacing (345 μm); (ii) small helix spacing (167 μm); (b) the different morphologies of the helical microfibrils observed after collection: (i) helical microfibrils with moderate helical spacing (379 μm); (ii) tightly packed spiral microfibers compared to loosely packed microfibrils. Reproduced with permission,[138] Copyright © 2021, American Chemical Society; (c) the helical fibers are cycled to 100% strain 100 times. Strain rate: 100 mm min^{-1}. Reproduced with permission,[139] Copyright © 2021, American Chemical Society.

the tensile cycle stability of the helical fibers (Fig. 22c).[140,141] In daily life, the elongation of human skin can reach about 55%.[142,143] The helical fiber recovers well under 100% deformation and has good cycle stability, which fully meets the deformation requirements of daily wearable devices. This work provides a scalable approach for high-strength hyper stretch and multifunctional fibers applied to wearable devices.

4.5. High strength of helical fibers

Nature has created many biomaterials with high strength and toughness, enabling living organisms to adapt to their natural environment.[144] For example, the stems of some plants can form a spiral structure spontaneously or under external influences[2] (Fig. 23a). These spirals have a high strength and can maintain a stable shape. At the same time, the spiral structure will show greater deformation under the action of external forces. As a result, this particular spiral structure gives the plant's stems both strength and toughness.[145] Inspired by this helical structure, nylon straight fibers are converted into helical fibers, and then they are introduced into silicone rubber (SR) to prepare composites.[146] There are great differences between helical fibers and straight fibers in terms of physical structure and mechanical properties (Fig. 23b). First of all, the linear fiber is a one-dimensional filler, and the helical fiber is a three-dimensional reinforcing material with variable parameters (helix angle, pitch, inner diameter, fiber diameter), and it can be found that the thread length is negatively correlated with the helix angle. As the pitch increases, the helix angle gradually decreases. The helix angle and pitch are related as follows:

$$\tan \alpha_c = \frac{P}{2D} \quad (1)$$

$$\alpha_f = 90^\circ - \alpha_c \quad (2)$$

where α_c is the angle between the spiral direction and the fiber cross-section, P is the pitch, D is the inner diameter of the helical fiber, and α_f is the helix angle.

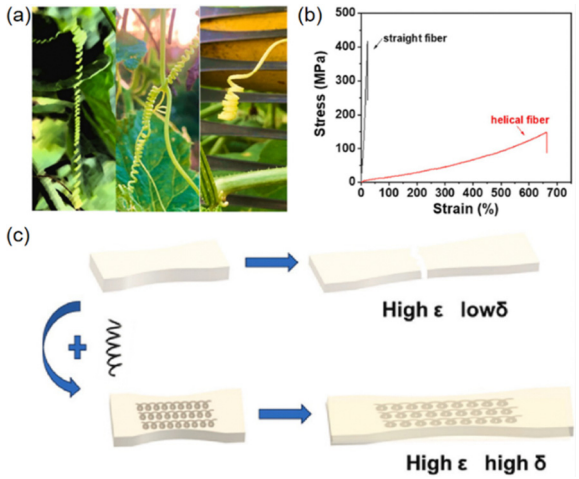

Fig. 23 (a) The natural spiral stem of the plant formed under external influences or spontaneously; (b) stress–strain curves of spiral and linear fibers; (c) schematic diagram of a helical fiber composite (ε and σ represent strain and stress, respectively). Reproduced with permission,[146] © 2024 Elsevier Ltd. All rights reserved.

As a result, the spiral parameters can be easily adjusted by means of the pre-stretch ratio as well as the fiber diameter and inner diameter. Secondly, the mechanical properties of helical fibers and straight fibers are different. Straight fibers have high tensile strength (~400 MPa) and small deformation (~18%). The helical fibers maintain high tensile strength (~200 MPa) and the elongation at break increases to 650%. These properties lead to a large deformation of the SR matrix under the action of external force (Fig. 23c). Therefore, when the composite material is subjected to an external force, the helical fiber can withstand the main stress as a "hard segment". In addition, the helical fibers can move synchronously with the SR matrix (soft segment), maintaining the original characteristics of the SR matrix with high deformation. As a result, helical fibers show a strengthening and toughening effect.[146]

5. Application of helical fibers

5.1. Optical field

In recent years, optical fiber torsion sensors have attracted the attention of various scholars. They have the advantages of low cost, easy manufacturing, and anti-electromagnetic interference, and are widely used in aerospace engineering,[147] geological health monitoring,[148] anthropomorphic robots,[149] and other fields. At present, several types of torsion sensors have been reported; these can be divided into two broad categories: torsion sensors based on fiber gratings and torsion sensors based on fiber optic interferometers. Torsional sensors based on fiber optic interferometers mainly rely on the change in the refractive index or birefringence of the fiber caused by torsion, which affects the interference spectrum. However, this type of torsion sensor suffers from the difficulty of identifying the direction of torsion. To solve this problem, interferometers with spiral or antisymmetric structures have been proposed. Many emerging jobs are based on helical twisted photonic crystal fibers (PCFs) with mass sensitivity and recognizable orientations. The PCF production process is complex and the proportion of qualified products is low, which is not conducive to the commercial production of sensors, so a strength-modulated directional torsion sensor based on spiral taper fiber is proposed. In addition, the sensitivity of the sensor can be improved by using a helical structure and an asymmetrical structure.

Therefore Song *et al.* proposed an optical fiber torsion sensor based on helical fiber (HTCF) and experimentally demonstrated that it can be used to measure both the torsion angle and the direction of torsion (Fig. 24).[150] The sensor consists of a section of HTCF and two single-mode optical fibers (SMFs) to form a Mach-Zehnder interferometer (MZI). The helical structure is achieved by pretorsion of a 1 cm long twin-core fiber (TCF). The measured transmission spectra for the SMF-TCF-SMF structure and the SMF-HTCF-SMF structure are shown in Fig. 24e. The solid black lines indicate the spectrum before pre-twisting, and the other solid lines are the spectrum after pre-twisting, at angles of 180°, 360°, and 540°. It can be determined that by introducing the helical (HS) structure, the interference pattern is more pronounced and the extinction ratio (ER) of the inclination angle is significantly enhanced. Chang *et al.* proposed and demonstrated a multi-order wideband mode converter in a toroidal fiber (RCF) employing multi-pitch chirped long-period fiber grating (LPFG), in which multiple tones are introduced into each chirp to further increase the bandwidth.[151] The theoretical and experimental grating parameters are optimized to generate broadband modes in OAM ± 2 and OAM ± 3

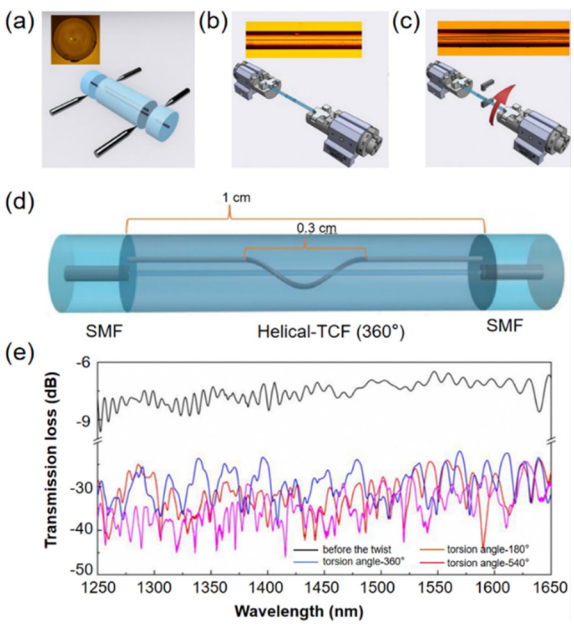

Fig. 24 The production process of the sensing structure. (a) Fusion splicing of TCF and SMF. (b) Keep the fibers straight. (c) Twisting and heating the TCF. (d) Schematic diagram of the sensing structure (360°). (e) Transmitted spectra of measured HS-free structures and HS-structured MZIs. Reproduced with permission,[150] © 1996–2024 MDPI (Basel, Switzerland).

modes by increasing the number of chirps and tones. The mode conversion efficiency is higher than 90% with a broadband of 57 nm from 1456 nm to 1513 nm and 51 nm from 1573 nm to 1624 nm, corresponding to the second-order OAM mode and third-order OAM mode, respectively.

5.2. Biotechnology field

Plasmonic nanoparticles (NPs) have been proposed as materials with great potential for biomedical applications, such as biosensing, drug delivery, or photothermal therapy.[152] Similar to the differential absorption of left and right circularly polarized light in optically active chiral molecules, such as DNA and proteins, strong CD signals can be generated by the coupling of plasma dipoles in chiral metal NP assemblies. Liz-Marzan and colleagues recently provided a good example of the strong optical activity of helically arranged gold nanorods (NRs), in which the origin of the surface plasmon CD (SP-CD) is aided by a coupled plasmonic dipole model, illustrating how helical nanoscale chirality can be used to detect protein aggregation, particularly amyloid fibril aggregation, which has been implicated in many neurodegenerative diseases.[153] They demonstrated that the assembly of Au NRs produces a chiral double helix arrangement on amyloid fibrils (Fig. 25a is a TEM image of the α synuclein fibrils), showing enhanced plasma crossover signal, indicating the presence of amyloid. The method was extended to detect infectious recombinant prions and α synuclein fibrils, suggesting a variety of possible disease-related targets.

There is also a class of systematically designed ultra-small (tri- to heptamer) peptides with minimal natural non-aromatic structures that can self-assemble into hydrogels in water.[14] The peptide motif consists of a tail of aliphatic amino acids with reduced hydrophobicity and a polar head at the top. Fiber scaffolds are assembled from nanostructured aggregates into concentrated three-dimensional (3D) grids that capture up to 99.9% of water and similar collagen fibers in the extracellular matrix. The resulting hydrogel is biocompatible, with heat resistance up to 90 °C, and exhibits tunable high mechanical strength. Due to the ease of synthesis and cost-effectiveness, these new materials will be used in applications ranging from injectable drug therapy to tissue engineering scaffolds.

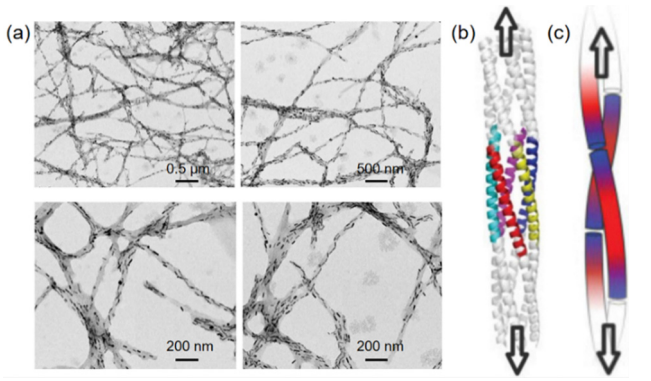

Fig. 25 (a) Representative TEM images of the sample produced by the addition of α-synuclein fibrils to gold nanorod colloids. Reproduced with permission,[153] © 2018. Published under the PNAS license; principle of fiber helix–helix assembly: (b) sliding assembly of the coil–coil pentamer (colored). Reproduced with permission,[154] Copyright © 2010 Wiley Periodicals, Inc; (c) interlaced coil–coil assembly to guide fiber assembly in peptide YZ1. Reproduced with permission,[155] Copyright © 2008, American Chemical Society.

One possible mechanism of fiber formation is the sliding of the hydrophobic surface of the amphiphilic helix to form a staggered assembly. Kajava and colleagues put it in a more robust design frame to make fibers based on the coil–coil pentamer.[154] The sequence αFFP thus designed, QLAREL $(QQLAREL)_4$, forms fibers under certain conditions, as shown in Fig. 25b. The group has followed this with redesigns and further characterization and the incorporation of N-terminal RGD-based sequences to promote cell adhesion. Conticello's group specified staggered coil–coil assemblies to guide fiber assembly in peptide YZ1, as shown in Fig. 25c.[155] This is characterized by the interaction of electrostatic bonds and buried hydrogen bonds between the helices, to cement the stagger and promote longitudinal growth.

5.3. Biomedical field

Three-dimensional (3D) helix structure is widely used in optics, nanotechnology, biotechnology, and biomedicine and has been shown to have unique optical and physical properties. Due to the chirality of the incident light and comparable geometric parameters (*e.g.*, pitch and pitch diameter) with the wavelength of the light,[156] the sharp chirality involved in the nano helix may interact with circularly polarized light in different ways, which can provide photodynamic helix structured nanofibers antimicrobial membranes by providing enhanced light absorption efficiency for efficient antimicrobial purposes. So, Hu *et al.* experimentally verified that CA/TPU-based helical fiber membranes are suitable and reliable for producing spiral structure fiber membranes with a consistent and controllable shape by applying CCD models.[157] The photodynamic helical fiber antibacterial film prepared by coaxial co-electrospinning exhibits the synergistic effect of APDT and antibacterial agents under normal light irradiation, as shown in Fig. 26a. Under the action of light irradiation for 20 min, the release rate of –OH was 98.22% and the release rate of hydrogen peroxide was 88.36%. The sterilization rates of *Staphylococcus aureus* and *Escherichia coli* were 99.9% and 99.7% (Fig. 26b), respectively.

The helical structure of the fiber can increase the absorption rate of light, thereby increasing the release rate and amount of reactive oxygen species (ROS) free radicals, and increasing the antibacterial rate, providing a new strategic direction for the design of sustainable biomedical antimicrobial protective materials. Wang *et al.* proposed a high-performance and low-cost artificial ligament that uses arranged carbon nanotube (CNT) sheets wrapped around spiral poly(ethylene terephthalate) (PET) fibers.[158] In the typical preparation of spiral composite fibers (HCFs), primary building fibers are obtained by uniformly wrapping CNT sheets on PET fibers. CNT sheets with arranged nanostructures are biocompatible and exhibit excellent mechanical properties. PET fiber is the most advanced synthetic ligament and is widely used in clinical practice. After twisting together

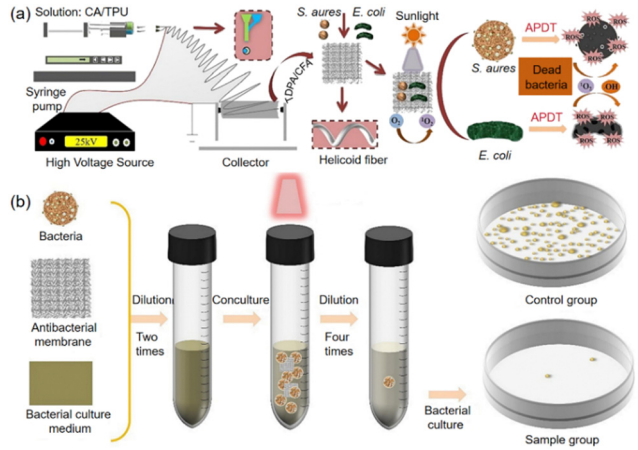

Fig. 26 (a) Preparation and antibacterial mechanism of the photodynamic helical fiber antibacterial film; (b) antimicrobial mechanism of the photodynamic helical fiber antibacterial film. Reproduced with permission,[157] © 2023 Elsevier B.V. All rights reserved.

multiple primary composite fibers, secondary helical fibers are obtained (Fig. 27a), which are equivalent to collagen bundles in the natural ligaments. HCF grafts were successfully fabricated by further twisting and folding the secondary helical fibers; Fig. 27b is an SEM image of a secondary composite fiber. The arranged carbon nanotube lamellae and helical structure give these artificial ligaments an anisotropic channel structure at the nano- and micrometer scales.

After implantation *in vivo*, these grafts encouraged bone regeneration and repair of bone tunnels in rats, and ultimately allowed the animals to stand, walk, and run with a normal gait (Fig. 27c). They have demonstrated that these ligaments can promote the regeneration of new bone and the effective repair of bone tunnels. These ligaments can also be continuously produced for further clinical applications.

5.4. Biomimetic structural materials

In the process of deformation and failure, there is a complex intralayer and interlayer stress distribution in the spiral structure, which has an important impact on the load transfer efficiency. As the interlayer helix angle changes, the stress distribution within and between layers will change significantly, which may lead to complex failure patterns (*i.e.*, fiber fracture, matrix fracture, fiber–matrix debonding, and spalling), which in turn will have a significant impact on the bearing capacity and energy absorption of the material. It has been shown that the shell of the hammer-like rod of the praying mantis shrimp is composed of oriented crystalline hydroxyapatite, amorphous calcium phosphate and carbonate multiphase composites. The helical structure (Bouligand structure) is a key factor on the material's energy dissipation and hindering crack propagation. Zhang *et al.* prepared a biomimetic structural material with excellent strength and toughness by imitating the spiral layered structure of mantis shrimp rods, using a carbon fiber/epoxy resin composite thin layer design, and studied its deformation and energy absorption properties.[159] It shows that the load-bearing capacity and energy absorption features of the Bouligand helical layered structure are closely related to the interlaminar helix angle. As the helical angle changes, the magnitude and distribution of stress within each single-layer structure and between adjacent layers will change significantly. These changes will have an important impact on the bearing capacity and failure form of each single-layer structure, as well as the load transfer efficiency and the spiral progressive failure of adjacent interlayer cracks in the laminate structure, thereby affecting the overall bearing capacity and energy absorption of the material. These results provide useful guidance for the design and performance optimization of lightweight construction materials.

The helical topology provides unique mechanical functions that can activate certain phenomena,[36] such as winding vines, and important cellular functions, such as DNA folding and packaging into chromosomes. The understanding of active mechanical processes in plants, certain muscle tissues in animals, and some biochemical processes in cells provides insights into the versatility of spirals. Most of these natural systems are made up of helically oriented filaments embedded in a compliant matrix. In some cases, the matrix can change volume, while in others, the filaments can shrink and the substrate is passive. In both cases, the spirally arranged fibers determine the overall shape variation, including length contraction/elongation, twisting, bending, and curling. Synthetic actuator materials and systems employing helical topologies have recently been described and demonstrate many fascinating and complex shape variations. However, significant new opportunities exist to mimic some of the most remarkable actions in nature, including the *Vorticella's* coiling stalk and DNA's supercoils, in the quest for superior artificial muscles.

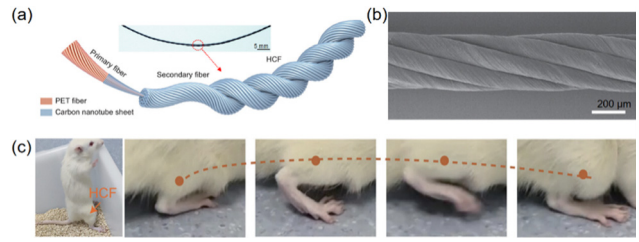

Fig. 27 (a) Schematic diagram of the structure of a HCF with a hierarchical helical structure, the illustration above is the photo of a HCF; (b) SEM image of a secondary composite fiber by twisting multiple primary fibers; (c) photographs of standing rats and their completed jumps two weeks after reconstructive surgery. Reproduced with permission,[158] © 2023 Wiley-VCH GmbH.

5.5. Sensor field

With the increasing commercialization prospect of various artificial intelligence electronic products, there is more and more research on wearable electronic devices in the fields of health monitoring[160] and intelligent robots.[161] Capacitive sensors are more popular due to their low power consumption, high sensitivity, and signal stability, and are considered simple and effective in wearable electronic devices to interact with the environment, primarily through physical contact or non-contact detection. In order to construct a practical and reliable

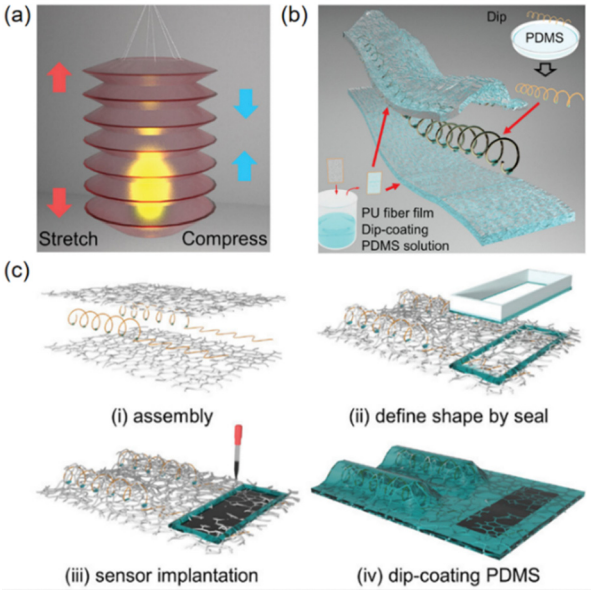

Fig. 28 (a) Schematic diagram of the structure of the accordion lantern; (b) schematic diagram of the exploded diagram of supradermal spiral interconnects (OSHI) and schematic diagram of the preparation method; (c) schematic diagram of the fabrication of an OSHI-based integrated sensor interconnect thin-film device. Reproduced with permission,[166] © 2023 Wiley-VCH GmbH.

wearable fiber optic capacitive sensor, excellent tensile deformation and dielectric material selection are essential.[162–165] A three-dimensional spiral on-skin interconnect introduces the first electronic sensor of the epidermis. Inspired by the structure of accordion lanterns,[166] the interconnection consists of two electrospun polyurethane (PU) fiber films and a spiral metal fiber, as shown in Fig. 28a and b. Helical metal fibers act as a stable conductor with stretchability, while PU fiber membranes with polydimethylsiloxane provide a self-adhesive substrate.

There is also a scalable preparation method to prepare an all-in-one sensor-connected strain measurement device. First, two spiral copper fibers are wrapped around an electrospun PU fiber film (Fig. 28c-i), which is the same process as mentioned in Fig. 28b; the only difference is that one end of the spiral copper fiber is flattened in preparation for subsequent sensor implantation. A hollow mold with the designed shape is then immersed in the PDMS precursor and pressed against the film like a seal to determine the shape and position of the sensor (Fig. 28c-ii). Here, a conductive coating of waterborne carbon nanotubes is used as an example to form a strain sensor film by drop-coating (Fig. 28c-iii). Finally, by dipping the film with PDMS, an integrated strain sensor was realized.

Besides, Liang *et al.* prepared BC@BC/CNT helical fibers with a skin core structure by a coaxial spinning and curling process, with biodegradable and insulated BC as the skin and conductive BC/CNT (BC : CNT = 1 : 2) composite materials as the core.[167] The BC@BC/CNT fiber has a core structure, high flexibility, strong mechanical properties, high conductivity, good wear resistance and scalability. As shown in Fig. 29a, helical fibers can be woven onto commercial gloves, and

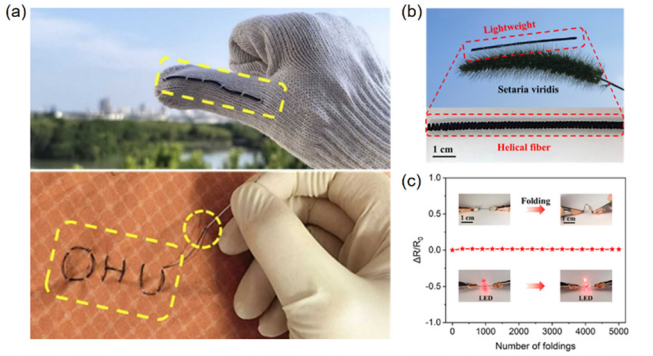

Fig. 29 (a) Long flexible BC@BC/CNT helical fibers woven with commercial gloves and straight fibers threaded through fine needles and pierced on cloth; (b) the lightness of BC@BC/CNT helical fiber; (c) effect of BC@BC/CNT straight fiber bending on conductivity. Reproduced with permission,[167] © 2023 Elsevier Ltd. All rights reserved.

straight fibers can be needle-punched, knotted, and sewn in textiles like commercial fibers, with a small diameter that has no aesthetic impact (280 μm). As shown in Fig. 29b, the helical fibers can be placed on t *Setaria viridis*, while the beard of Setaria viridis does not need to be bent, which confirms that our helical fibers are smaller and lighter. When the BC@BC/CNT straight fiber was bent 5000 times and the helical fiber was stretched to 300% (Fig. 29c), there was no significant change in the brightness of the LED, proving that the conductivity had little to no effect, and that the helical fiber with the epidermal core structure could avoid the unwanted effects caused by resistance changes and signal interference when used in capacitive sensors.

5.6. Filtration applications

The global shortage of freshwater resources has led to the rapid development of membrane desalination processes for producing clean water to meet the needs of industry and households. Although membrane filtration is superior to traditional treatment processes in terms of final product quality, fouling is still an unavoidable problem, which significantly reduces the efficiency of the filtration system.[168] To reduce fouling load (by achieving compactness in a cross-flow setup), most reverse osmosis (RO) and nanofiltration (NF) membranes, as well as some microfiltration (MF) and ultrafiltration membranes, are arranged in a spiral wound configuration so that the diaphragms are sandwiched between spacer structures.

In Sarah Kerdi's study, they developed simple and practical helical structures with one, two, or three helixes per filament to take advantage of their ability to generate additional vortices near the membrane surface.[169] The generation of these vortices inherently mitigates pollution and increases the generation of permeate fluxes. They are designed using computer-aided design (CAD) and produced using 3D printing technology, as shown in Fig. 30a. They were further evaluated in well-controlled experimental conditions with respect to permeate flux decline and fouling mitigation during the (bio)fouling development. Fig. 30b shows the change in the specific

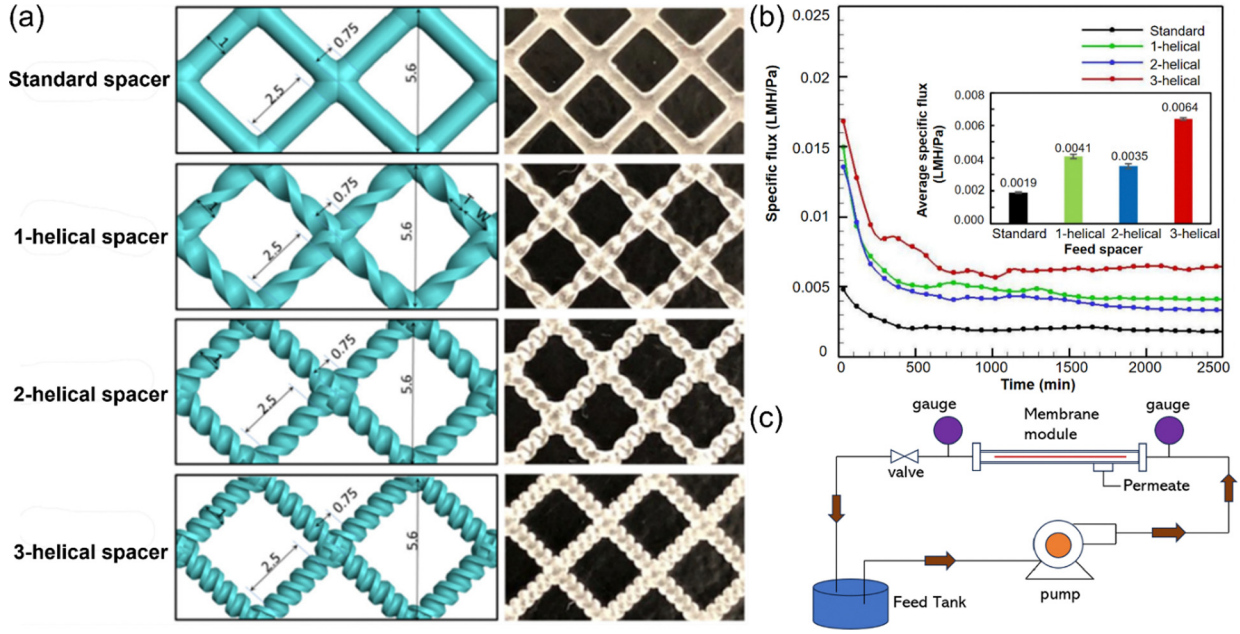

Fig. 30 (a) Design of the spiral spacer. CAD (left, size in mm) and digital photographs (right) as well as standard and spiral spacer dimensions; (b) average specific permeate flux at steady-state filtration (inset) and percentage of flux recovery relative to standard spacer as a function of the number of helices in the spacer structure. Reproduced with permission,[169] © 2020 Elsevier B.V. All rights reserved; (c) schematic diagram of the experimental setup for membrane filtration. Reproduced with permission.[170]

permeate flux of the spiral gasket during filtration. The variation of the pressure drop of all spacer layers with different velocities in the channel was studied. The effect of helix count on process performance was also examined, and the observed trend was compared to the trend of using helix-free intervals (known as standard intervals) for filtration experiments. Then they further applied advanced direct numerical simulation (DNS) techniques to elucidate the mechanism and key parameters, which highlighted the improved performance of the spiral spacer in membrane filtration operations. Kuakuvi *et al.* compared the performance behavior of spiral hollow fibers and straight hollow fibers in running some ultrafiltration experiments.[170] The membrane module consists of 20 fibers, corresponding to a total membrane area of 2.05×10^{-2} m^2. The inner fiber diameter is 0.7 mm, and the fiber length is 470 mm. As highlighted in the above study, the pressure drop is expected to be lower for the linear hollow fiber geometry, mainly due to the Dean vortex. However, these researchers determined that the larger the coil diameter (fiber) of the spiral membrane, the lower the pressure drop. In addition, membrane modules constructed with helical fibers have the highest permeation flux for similar levels of energy consumption. In the case of bovine serum albumin (BSA) filtration, spiral hollow fibers and straight hollow fibers were compared. The experimental filter settings are shown in Fig. 30c. The membrane permeability of spiral hollow fibers for pure water filtration is 227 L h^{-1} m^{-2} bar^{-1}, which is 72% higher than that of straight hollow fibers.

5.7. Soft robots

Soft pneumatic robots have attracted much attention as a promising alternative to hard and rigid robots due to their deformability, flexibility, low cost, and good environmental compatibility.[171] They are of particular interest in areas involving human interaction and fragile objects. The design of soft robots is often inspired by living organisms that move around and adapt to their surroundings. With recent developments in pneumatic technology, soft materials, and high-precision motion control, the field of soft robotics has made significant progress. While complex soft robots can achieve comprehensive movements, they often require multiple coordinated pneumatic controls to achieve the simplest movements. In addition, most soft robots lack the ability to perceive the environment and provide feedback to the pneumatic control system. Advances in plant-inspired robotics, particularly in tendril-inspired soft robotics, have enhanced the derivation of functions that adapt to plant behaviors that will have a significant impact on environmental applications, and several robots and actuators have been developed that mimic tendril-like curling behavior through the use of interactions between materials and structural arrangements.[172] The tendril-shaped soft robot proposed by Meder *et al.* is based on a "programmed" material that has a state of equilibrium in a helical spiral structure.[173] This can be achieved by tightly binding the elastomer layers in different stretch/stretch states, resulting in a structure similar to asymmetrically shrunken tendril fibers. Two silicone elastomer layers, one uniaxially stretched and one still in a relaxed state, are bonded together and constrained by the interaction between the stretched and relaxed layers to form a helical structure. The result is a spiral-curled structure of the bilayer material spontaneously forming in equilibrium. Now, in order to control the winding, the winding force is overcome by adding a stiffer core, which prevents the winding force, resulting in a physically straight material, which throws the bilayer material out of balance. Researchers

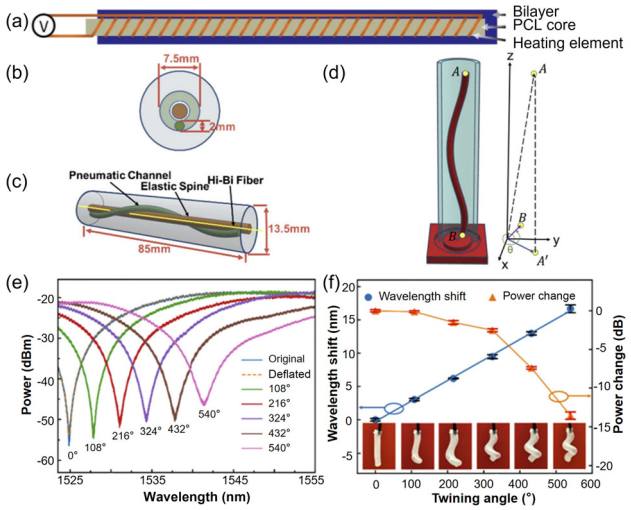

Fig. 31 (a) A simple structural schematic diagram of an artificial tendril that mainly uses the physical properties of the integrated material to control the tendril. Reproduced with permission,[173] © Copyright 2024 IEEE; (b) top view of the soft spiral gripper; (c) 3D view of the soft spiral gripper; (d) 3D printed molds for the manufacture of soft spiral grippers; (e) interferometric spectra of embedded HiBi fiber optic sensors in a Sagnac configuration; (f) effect of the winding angle on the HiBi fiber optic sensor embedded in the screw gripper – wavelength shift (blue) and power change (orange). Reproduced with permission,[174] © Copyright 2024 | Optica Publishing Group.

chose a 3D printed thermoplastic polycaprolactone (PCL) rectangular rod as the core material (Fig. 31a), which is also used as a phase change element. The advantage of PCL is that it is a biodegradable polyester with a melting point of about 60 °C. Thus, at relatively low temperatures, its phase transition from solid to liquid can be triggered. In the solid state, the size of the PCL rod can withstand the forces exerted by the elastomer bilayer. However, when transitioning to the liquid state, the PCL core no longer balances the forces applied by the elastomer constraints, allowing for winding. Mei Yang *et al.* designed a soft robotic spiral gripper inspired by a wound plant that requires only one pneumatic control device to perform the winding motion and firmly grasp the target object,[174] as shown in Fig. 31. The soft robot spiral gripper features an embedded high birefringence fiber optic twist sensor that provides critical information, including the angle of winding, the presence of external disturbances, and the physical parameters of the target object.

As shown in Fig. 31b and c, the soft spiral gripper consists of a cylindrical elastomer (light gray) made of silicone rubber to carry the spiral pneumatic channel (green) for winding motion, and the HiBi fiber sensor (yellow) is embedded in the elastic spine (brown) to eliminate delamination of the fiber optic sensor. As shown in Fig. 31e, a wavelength shift of 16.66 nm is observed when the winding angle of the soft spiral gripper increases from 0° to 540°. The relationship between the meshing angle and the wavelength shift of the Sagnac loop spectrum is then measured, as shown by the blue data point in the figure. Fig. 31f yields a first-order fitting line with a slope of 0.03 nm per °, which can be used to represent the winding sensitivity of the HiBi fiber sensor. The experiment is repeated five times to measure wavelength shifts and power changes due to changes in winding angles. The deviation of the measured value is plotted as error bars. Small errors are observed, which proves that both the screw gripper and the embedded HiBi fiber sensor have high repeatability.

Most multi-robot operations are limited to rigid body and colloidal particle systems. Untethered, battery-free motion control of soft robot groups remains a challenge due to the complex coordination required for each individual movement.[175,176] Won *et al.* proposed a new method for manipulating multiple soft robots that are regulated by a single axial magnetic rotation below the center of the substrate.[120] The Spinbot is a self-contained soft robot that rotates in layers around the center of the substrate by a rotational motion. The three different modes in rotational motion, namely rotating, pivoting, and tumbling, are controlled by varying the magnetic rotational speed. With the orbital control of these three rotation modes, it is possible to select the desired track with independent speeds in the multi-body drive. Orbital motion demonstrates the adaptability of conformal motion, which bypasses blocked paths and magnetic dynamics in land and water environments, and is suitable for multiple collective soft robotic systems.

5.8. Helical fiber composites

Nature is an incredible resource that offers potential solutions to fundamental problems such as matter, force, and heat transfer in man-made materials mentioned above. An example is procollagen (Fig. 32a). Its basic building block, three amino acid chains, is organized into collagen fibers and tendons in the form of three coils. This typical procollagen helical structure can successfully extend the one-dimensional mechanical advantages of macromolecular chains to three-dimensional energy dissipation and crack propagation inhibition, providing significant mechanical toughness to tendons.[177] Applying the above 3D force propagation in the tendon, herein, we have successfully extended the 1D thermal conductive feature of oriented polymer fibers into the 3D space by processing high-k PBO fibers into a spiral structure and weaving them into an

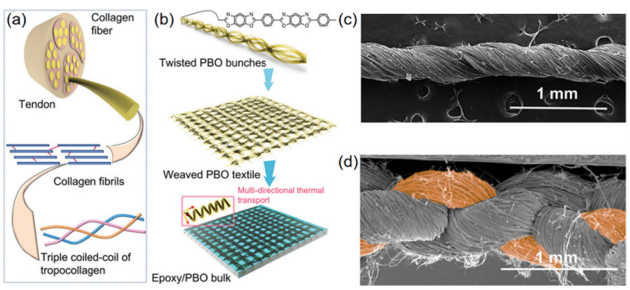

Fig. 32 (a) The scheme of describing the hierarchical organization of tendons from the macroscopic to the molecular scale, with three amino acid chains arranged in a three-curly basic configuration; (b) schematic diagram of the synthesis of 3D thermally conductive epoxy/PBO bulk materials from macromolecule selection to microstructure; (c) SEM image showing distorted PBO fiber bundles; (d) SEM image showing a cross-sectional view of a woven PBO textile, a bundle of PBO fibers is shown in orange. Reproduced with permission,[178] © 2022 Wiley-VCH GmbH.

epoxy matrix. The epoxy/PBO bulk material was tailored through a bottom-up approach (Fig. 32b), including rational molecular selection of a polymer, engineering the polymer into a continuous and highly oriented fiber, twisting the fibrous bunches into the spiral structure, weaving the spiral fibers into a textile, and vacuum impregnation of epoxy precursors to fabricate the epoxy/fiber bulk. Considering the prerequisites for insulation application and torsion process, the authors selected an aromatic polymer PBO with excellent electrical insulation and significant mechanical properties as the basic building block. In Fig. 32c, the scanning electron microscope image shows that the one-dimensional thermal conductivity of the PBO fiber can be extended to multiple directions by the twisting method by successfully cutting the one-dimensional PBO fiber into a helical structure. After twisting, the PBO bundles are woven into a plain weave fabric with the bundles woven up and down (Fig. 32d), which further adjusts the thermal conductivity according to the weave density. Unlike aliphatic or other aromatic polymers, PBOs contain linearly symmetrical fragments while avoiding strong interchain interactions (*i.e.*, hydrogen bonding), which prevents additional phonon scattering from the side chain and interchain vibrational modes from the longitudinal phonon along the chain axis. Therefore, PBO can theoretically exhibit high k at the molecular level and good thermal stability. In order to maintain its theoretical heat transfer advantage in the form of one-dimensional fibers, liquid crystal spinning and drawing methods are well-established industrial techniques for processing PBO chains into extended molecular configurations.[178]

The aim of this *in vitro* study was to investigate the compressive strength and the bulk porosity of a bidirectional (bFRC) and an experimental bidirectional spiral winding reinforced fiber composite (bswFRC). Cylindrical specimens were prepared for each material group and treated in distilled water at 37 °C under different storage conditions (dry, 1 and 3 months) to assess the compressive strength. The degree of volumetric porosity of the specimen was assessed by X-ray tomography. Scanning electron microscopy (SEM) was used to determine the fracture mode.[179] Data were statistically analyzed using two-way analysis of variance (ANOVA). Under dry conditions, the compressive strength of the bFRC sample was significantly lower than that of the bswFRC sample after 1 month of water immersion ($p < 0.05$). There was no significant difference between the two groups after 3 months of immersion ($P > 0.05$). However, the presence of water seriously affects the compressive strength of bswFRC after water storage. The types of fractures were significantly different between the two groups: bswFRC showed severe fractures, while bFRC showed shear fracture. The pore volume density of bswFRC is higher than that of bFRC. In summary, bswFRC has greater compressive strength under dry conditions, but water aging can significantly reduce the mechanical properties of this innovative FRC. Therefore, both the new bidirectional spiral winding reinforced fiber composites (bswFRC) and bidirectional fiber reinforced composites (bFRC) may be suitable materials for post-production and core systems by CAD/CAM technology. These findings suggest that both FRC materials have the potential to strengthen the root canal-treated teeth.

5.9. Refrigeration applications

The development of high-efficiency solid-state cooling technologies and high-cycle life materials is a top priority. Polyethylenedioxacyclopentene (PBO) is a high-performance fiber with excellent mechanical properties. Feng *et al.* reported for the first time elastic and twist cooling of PBO fibers by stretching and twisting PBO fiber bundles.[180] The incomplete crimp structure cannot ensure the uniformity of the fiber structure, and the temperature change will not be uniform, which affects the accuracy of the measurement results. If too much twist is applied after the fiber bundle has fully formed a coil structure, the fiber bundle will break, so the PBO fibers are twisted until a uniform coil structure is formed. As shown in Fig. 33a, the self-winding PBO fiber bundle is stretched and then the temperature of the fiber bundle increases. After that, the fibers remain in this state until the temperature returns to room temperature, and then the fiber bundles are released to return to their original length, at which point the temperature of the fiber bundles decreases. The temperature variation of the entire process is shown in Fig. 33b.

Closely related processes are applied to a wide range of yarn types, from carbon nanotube (CNT) yarns to polymer yarns and fibers. Similarly, the effect of yarn twist *versus* the relative chirality of yarn winding has a similar consequence on these different applications. Despite the variety of applications, similar manufacturing methods and associated mechanisms are

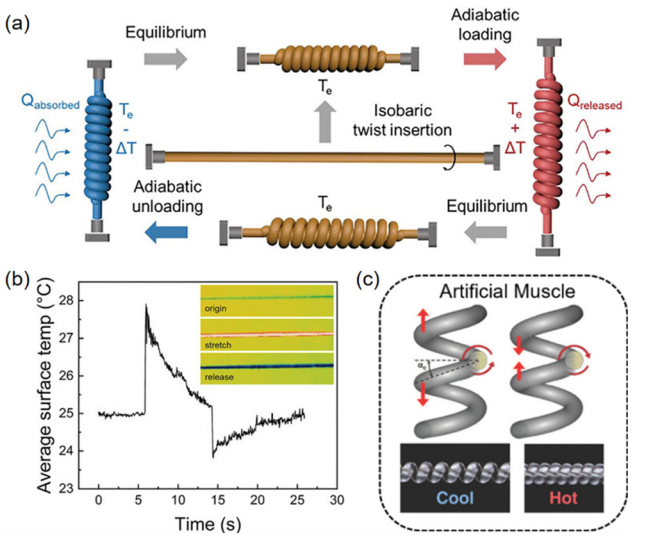

Fig. 33 (a) Schematic diagram of a self-winding PBO fiber bundle inserted into an isobaric twist to form a self-winding PBO fiber bundle for a cycle of stretch-induced heating and stretch-release-induced cooling; (b) temperature change over time during stretching and stretching release of a self-coiled PBO fiber bundle with a spring index of 1.78. The inset shows the thermal image of a self-winding PBO fiber bundle stretched and stretched after release. Reproduced with permission,[180] © 2023 Wiley-VCH GmbH; (c) highly reversible yarn is used for refrigeration Reproduced with permission,[181] Copyright © 2023, © SAGE Publications.

used to provide vast, highly reversible yarn elasticity as well as associated performance variations that lead to muscle drive, energy harvesting, and cooling (Fig. 33c).[181]

5.10. Helical fiber filling

Helical fiber filling is a special filling material, usually made of nylon, polypropylene, and other materials with a spiral-shaped fiber structure. The helical fiber filling has a unique structure and can be divided into two shapes: comb and wave. This filler has a compact structure and a large surface area, which is conducive to dispersing and shaping gases and improving gas–liquid mass transfer. Helical fiber fillers are widely used in industry, agriculture and environmental protection and other fields, mainly including the following aspects. At the same time, they also have the following effects:

(1) Increase the contact area: the surface area of the helical fiber filler is much larger than that of the traditional filler such as gravel and plastic balls, which can increase the contact area between water and air, thereby improving the mass transfer effect between gas and liquid.

(2) Anti-blocking performance: the spiral shape of this type of filler helps the flow of water inside, thereby reducing the resistance inside the filler and greatly extending the service life.

(3) Purification treatment: helical fiber filler is suitable for the process of water purification, which can effectively adsorb harmful substances in the water body and improve the purification effect of the water body.

5.10.1. Sewage treatment. With the development of industry and the growth of population,[182–187] water pollution has become a prominent global problem.[188–191] The safety of drinking water, as well as all water resources for which drinking water is actually or may be earmarked, needs to be assessed to ensure public health.[192] In order to improve the detection sensitivity of trace volatile organic compounds in water, a new inlet ionization source of spiral membrane was designed. Fig. 34a is a schematic diagram of the source of single-photon ionization (SPI) of a spiral hollow fiber membrane. The membrane is spirally wound in the ionization source, and the pressure in the ionization source increases to 28 Pa as the membrane surface area increases. The sample input through the semipermeable membrane reached 6 mL min^{-1}, a 30-fold increase over the 1 Pa in the SPI source.[193] A newly designed four-stage differential vacuum TOFMS is used to maintain high pressure inside the SPI source. The effects of sampling speed, membrane length and temperature on MIMS sensitivity were studied. In addition, the response time of the membrane inlet under different conditions was compared. Finally, SPI-TOFMS was used to automatically monitor volatile organic compounds (VOCs) in laboratory construction wastewater.[194] The wastewater in the biological laboratory building was then automatically monitored for 24 hours and the changes in the concentrations of benzene, paraxylene, and chlorobenzene (MCBz) were monitored, as shown in Fig. 34b. The concentrations of benzene, paraxylene, and MCBz vary continuously throughout the day and should be related to laboratory activities. The maximum concentration of benzene is 118 μg L^{-1}, which is above the discharge threshold of 100 μg L^{-1} issued by the Chinese National Standards (CNS) for comprehensive wastewater discharge. This means that the biological laboratory building should be equipped with a sewage treatment plant for further purification. Therefore, SPI-TOFMS can continuously and real-time monitor sewage, which is of great significance for observing the dynamic changes of pollutant concentration and quickly finding the pollution source.

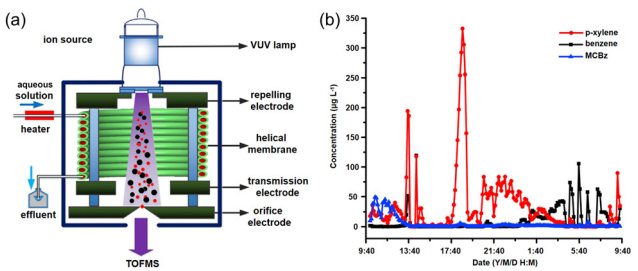

Fig. 34 (a) Schematic diagram of a single-photon ionization (SPI) source for a spiral hollow fiber membrane within the source; (b) the sewage of biological laboratory building was continuously monitored for 24 h. Reproduced with permission,[194] © 2018 Elsevier B.V. All rights reserved.

5.10.2. Air purification. With the development of social economy, residents' requirements for residential interior decoration are getting higher and higher. The use of large-scale decoration materials and building materials makes the concentration of pollutants such as formaldehyde and total volatile organic compounds (TVOC) in indoor air exceed the standard, which has an impact on people's health, immunity and other aspects.

Zhang *et al.* used a two-step morphology control strategy to design and fabricate a multi-efficiency zein-based fiber membrane with multi-level three-dimensional structure.[195] The preparation diagram is shown in Fig. 35a. Dual-solvent electrospinning makes the zein fiber membrane have a helical fiber structure, which promotes the formation of a three-dimensional fluffy structure with high porosity and large surface area, making the filter more efficient and less resistant in the air filtration process. In addition, due to the helical shape of the fibers and the loading of ZIF-8, multi-level structural membranes with microscale and nanoscale pores were prepared, which significantly increased the specific surface area and pore volume of zein membranes. In addition, solvent fumigation welding regulates the fiber surface, resulting in an increase in the exposure of ZIF-8 on the fiber surface, resulting in stronger adsorption of various contaminants. At the same time, welding adjacent zein fibers during solvent fumigation can potentially improve the mechanical properties of zein membranes. The green antibacterial zein fiber membrane has the characteristics of efficient $PM_{2.5}$ filtration, formaldehyde degradation and enhanced mechanical properties under low air droplets, and has a broad application prospect in air remediation to adapt to the sustainable development of the future. In order to understand and interpret the excellent filtration performance of the resulting membranes, the possible mechanisms by which morphology and composition contribute to the filtration performance were further analyzed (Fig. 35b). The abundant functional groups on

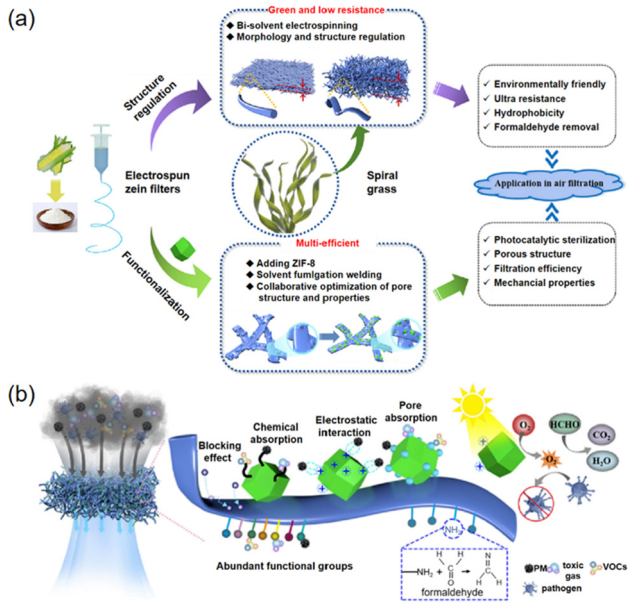

Fig. 35 (a) Schematic diagram of the preparation of zein-based nano-air filters by electrospinning different types of zein solutions and surface treatments; (b) proposed air pollutant capture mechanism. Reproduced with permission,[195] © 2023 Published by Elsevier B.V.

the surface of zein fibers can greatly promote the strong interaction between the filter and air pollutants, enabling the filter to efficiently remove PMs and chemical gaseous molecules.

5.10.3. Water purification. As an emerging field of soft matter science, supramolecular gels based on low molecular weight gelling agents (LMMGs) have attracted increasing attention in the past few decades, and many molecular gels with fascinating properties have been reported. LMMGs and related molecular gels have recently been used for water purification due to their convenience and high efficiency, but the process is time-consuming due to the limited two-phase contact and low extraction efficiency. Yan *et al.* specifically designed two novel dicholesterol-based gelling agents containing ferrocene units, 1 and 2, and most of the gels containing 2 prepared by heating–cooling cycles are intelligently thixotropic.[196] Specifically, for the 2/heptane gel system, the shear-induced sol–gel phase transition is fast (in a few seconds) and the filling model of gelling agent 2 in its heptane gel is shown in Fig. 36a. And it is completely reversible at room temperature. Using thixotropic gels, a new wastewater purification strategy with high liquid–liquid extraction efficiency and convenient liquid–solid separation was proposed (Fig. 36b). After shaking vigorously by placing 0.34 g of 2/heptane gel in 3 mL of saturated I_2 aqueous solution, the mixture becomes a viscous emulsion. However, the 2/heptane gel recovers immediately after a short rest (less than 2 minutes). At the same time, the water layer became clear, indicating that I_2 was efficiently extracted from the aqueous phase to the gel phase. Then, the residual gel was removed by filtration. It is believed that the research in this work will attract extensive attention to water purification and is of great significance for enhancing the practical application of LMMG-based molecular gels.

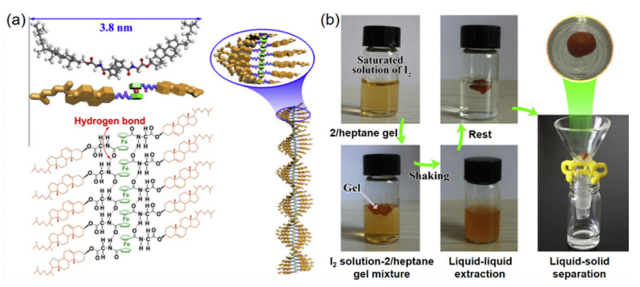

Fig. 36 (a) Schematic diagram of the self-assembly behavior of gelling agent 2 in heptane; (b) adsorbed I2 is extracted from water by a 2/heptane gel. Reproduced with permission,[196] Copyright © 2015 Elsevier Inc. All rights reserved.

5.10.4. Energy storage filling. As a promising energy storage material, spiral carbon fibers (HCFs) have attracted extensive attention due to their unique form and superior performance. However, the easy synthesis of HCFs with high spatial surface area (SSA) and good electrochemical properties remains a challenge. Zhu *et al.* used spiral containers (HVs) extracted from tea as biological templates, and synthesized HCFs using a catalyst-free strategy, and further obtained spiral porous activated carbon flakes (HPACFs) by potassium hydroxide activation.[197] Fig. 37a shows the carbonization and activation process of spiral carbon. The prepared HPACFs had a high SSA (3124 $m^2\ g^{-1}$), good pore structure, rapid migration of electrolyte ions and electrons, and good electrochemical energy storage performance. The specific capacitance of the prepared HPACFs in the two-electrode system was 187 F g^{-1} (1 A g^{-1}),

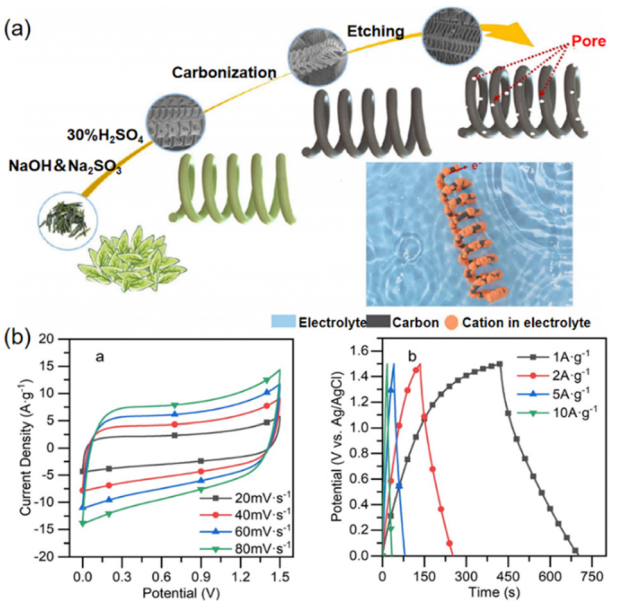

Fig. 37 (a) Schematic diagram of spiral porous activated carbon sheets (HPACFs) obtained; (b) CV curves at different scan rates; (c) GCD curves at different current densities. Reproduced with permission,[197] Copyright © 2022, The Author(s), under exclusive licence to Springer-Verlag GmbH Germany, part of Springer Nature.

and the cycling stability was good (7% loss after 3000 cycles at 20 A g^{-1}). The spiral porous structure provides a combination of defect sites and nanoporous regions, optimizing electrolyte ions and energy storage devices. In addition, large SSAs can provide sufficient active sites for ion storage and improve ion diffusion. Its high capacitance and long-term stability indicate that it has good advantages for next-generation hybrid energy storage and renewable energy devices. Fig. 37b shows the CV curves of the HPACF-5 tested in a two-electrode symmetrical aqueous SC configuration at different scan rates and GCD curves at different current densities. The quasi-rectangles in the CV curve and the relatively symmetrical triangles in the GCD curve both indicate the characteristic behavior of the EDLC. In addition, the specific capacitance of HPACF-5 at 1 A g^{-1} can be calculated to be 187 F g^{-1}. HPACF-5 has a well-developed porous structure and high SSA, which can provide abundant active sites for ion adsorption and efficient formation of electric double layers, which is conducive to obtaining excellent electrochemical performance.

5.11. Electromagnetic shielding

The helical carbon fiber (HCF) is a new type of carbonaceous material, which has the characteristics of spiral morphology, chirality, and high conductivity. Compared with traditional carbon materials, the spring-shaped HCF exhibits different interactions and stronger electromagnetic wave absorption capacity to electromagnetic waves,[198] so helical fibers have the performance of microwave absorption, and chirality is an electromagnetic property that promotes asymmetric polarization, which is expected to achieve broadband absorption of microwave absorbing materials (MAMs). Therefore, Huang *et al.*, inspired by the microstructure of *Nepenthes* spp., reported a scalable preparation method for multi-level chiral spiral carbon fibers with broadband microwave absorption and multispectral chiral modulation.[199] A chiral barrier is established by applying a spirally distributed stress to the fiber, and a helical electric dipole is induced by the positive and negative charges accumulated at the barrier. In achiral, unichiral, and bichiral samples, the polarization loss states of Debye relaxation were 2, 3, and 4, respectively. The polarity vector of the achiral electric dipole is converted into a pseudovector by the chiral barrier to improve the synergistic magnetic loss, and the chiral grade is quantified based on the symmetry failure theory. The maximum absorption peak of −96.50 dB was reached at 30.67 GHz (2 wt% carbon) for unidirectional fibers, and the effective absorption bandwidth (RL ≤ −10 dB) for bichiral fibers was 8.8–18 GHz. In addition to microwaves, chiral photon manipulation also plays an important role in the near-ultraviolet and visible spectrum. The results of this study open up a new way for microwave absorption mechanism and integrated application using the chiral model.

Meanwhile, Ren *et al.* proposed a new strategy for the synthesis of chiral small molecule soft templates of supercoiled chiral polypyrrole nanofibers (Fig. 38a), which can be developed as a promising high-performance anticorrosive microwave absorber.[200] Due to supramolecular chiral-induced electromagnetic cross-polarization enhanced dielectric losses and additional magnetic losses, spiral polypyrrole nanofibers (HPPy) were found to enhance impedance matching and electromagnetic wave attenuation capabilities. In order to explain the electromagnetic wave absorption mechanism of spiral polypyrrole more clearly, a typical helical structure model is constructed to assist the explanation, as shown in Fig. 38b. The basic characteristic of chiral materials is the cross-polarization of the electromagnetic field. For chiral materials with a helical structure, there will be cross-polarization of the electromagnetic field in addition to the self-polarization of the electromagnetic field. When an electromagnetic wave is incident on a chiral material with a helical structure, not only Debye polarization and conductance loss are generated, but also an induced electric field and an induced magnetic field are generated. At the same time, the cross-polarization of the electromagnetic field will further enhance the ability of the material to lose electromagnetic waves.[201]

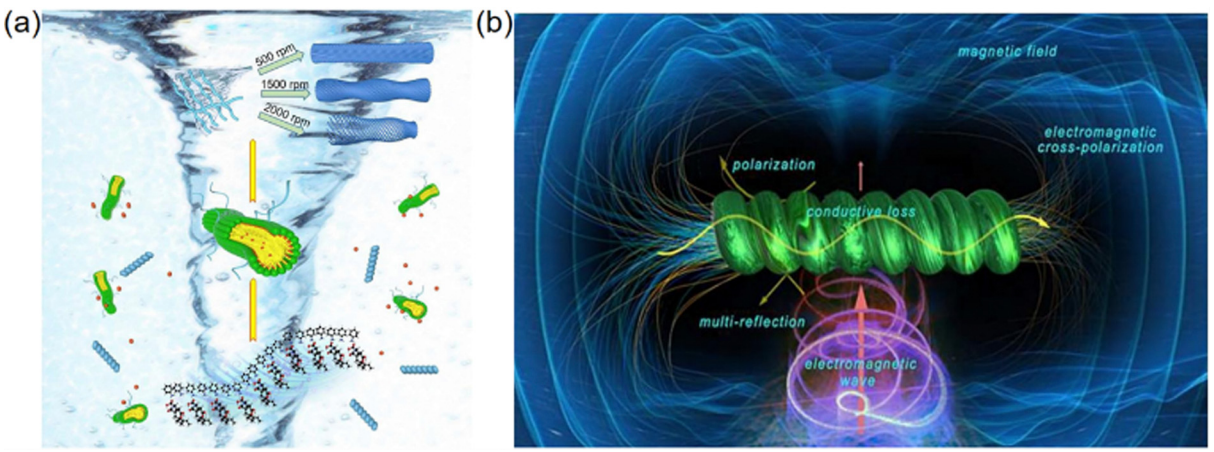

Fig. 38 (a) Synthesis mechanism of spiral polypyrrole nanofibers; (b) schematic diagram of the HPPy microwave absorption mechanism. Reproduced with permission,[200] © 2021 Elsevier B.V. All rights reserved.

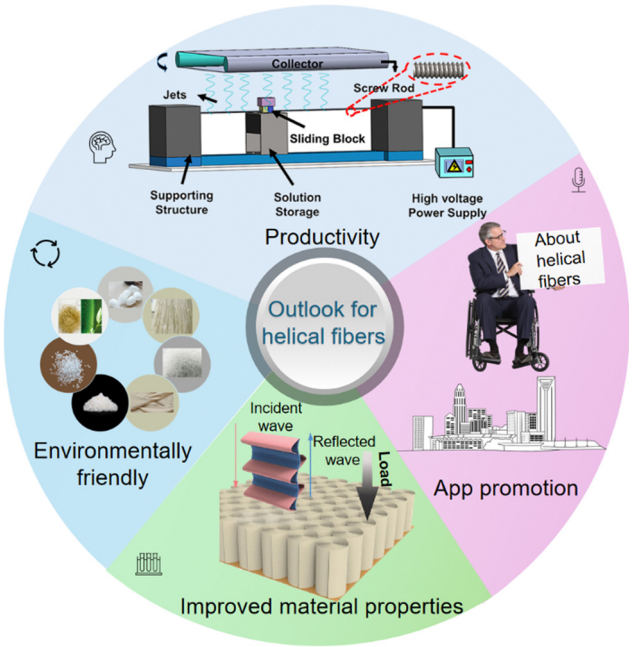

Fig. 39 Some solutions are currently available to promote the development of helical fibers. Reproduced with permission,[202] Copyright © 2024 American Chemical Society; reproduced with permission,[203] © 2024 The Authors. Advanced Science published by Wiley-VCH GmbH.

6. Conclusions and perspectives

Inspiration from biological systems has been a productive approach to many technical problems. By combining the best of materials science with an understanding of how nature solves similar problems, it is possible to devise new methods to produce materials with different properties. A spiral is a clever shape that is commonly found in nature. It provides additional flexibility and cohesion to the material, as well as the possibility of developing movement strategies. Therefore, it is natural for researchers to strive to tailor these shaped filaments to give the material favourable macroscopic properties. Helical fiber is a fiber with a unique morphological structure, and its surface presents a coiled or twisted shape similar to that of a spiral. This special structure gives the spiral fiber unique physical and chemical properties, making it have a wide range of application potential in textile, medical, materials science and other fields. Spiral fibers can be prepared in a variety of ways and can be achieved through specific spinning processes or post-processing techniques.

(1) From the perspective of materials science, there is still a lot of room for development in the preparation technology and performance optimization of helical fibers. For example, by controlling the spinning process, it is possible to produce helical fibers with better properties, such as higher strength, better electrical conductivity or higher thermal stability. In addition, the weaving and processing technology of helical fibers also requires further research and development to meet the needs of different application fields.

(2) From the perspective of application, helical fibers have great potential in the fields of wearable electronics and multifunctional weaving equipment. For example, they can be used as stretchable temperature sensors and gas sensors to detect high temperatures close to 300 degrees Celsius and harmful gases such as nitrogen dioxide and ammonia. This application not only improves people's quality of life, but also contributes to environmental protection and public safety.

However, despite the many advantages of helical fibers, there are still some challenges in practical applications: for example, how to maintain the stability of their performance in large-scale production, how to reduce production costs, how to dispose of and recycle waste helical fibers, *etc.* These issues require researchers and engineers to work together to achieve sustainable applications for helical fibers.

Fig. 39 provides some strategies to address the above problems that limit the widespread use of helical fibers. For example, more efficient production processes can be researched and developed, such as the use of advanced automotive equipment and process optimization, to reduce production costs and improve production efficiency. In addition, the performance of helical fibers is improved and optimized by strengthening, modifying or other means, such as improving the strength, heat resistance, chemical resistance, *etc.* Adopt environmentally friendly production processes and materials, and use them in an environmentally friendly way, reducing waste and pollutant emissions in the production process, while encouraging the recycling and reuse of helical fiber products for sustainable applications. In addition, increase investment in the R&D and innovation of helical fiber technology, encourage scientific research institutions and universities to carry out relevant research, and promote the continuous development and innovation of helical fiber technology. It can also strengthen marketing and promotion to improve public awareness and acceptance of helical fibers. At the same time, cooperate with related industries and fields to promote the application of helical fibers in various fields.

To sum up, the unique properties of spiral fiber will make it suitable for application in more fields, such as aerospace, electronic information, medical, *etc.* Because it is lightweight, flexible, of high strength, electrically conductive, thermally conductive, and can be weaved, it has broad application prospects in the fields of multifunctional fibers, functional composite materials, sensing, wearable displays,[204] and smart materials.[205] However, further research and development is needed to achieve its wide application in various fields. At the same time, we also need to pay attention to the challenges that may be faced in practical applications and seek solutions to achieve sustainable use of helical fibers.

Data availability

Data availability is not applicable to this article as no new data were created or analyzed in this study. The data in this article are derived from references.

Conflicts of interest

There are no conflicts to declare.

Acknowledgements

This work is financially supported by the National Key Research and Development Program of China (2022YFB3807300).

References

1 W. R. Davis, R. J. Slawson and G. R. Rigby, *Nature*, 1953, **171**, 756.
2 D. Brüggemann, J. Michel, N. Suter, M. Grande De Aguiar and M. Maas, *Beilstein J. Nanotechnol.*, 2020, **11**, 991–999.
3 Y. Li, F. Guo, Y. Hao, S. K. Gupta, J. Hu, Y. Wang, N. Wang, Y. Zhao and M. Guo, *Proc. Natl. Acad. Sci. U. S. A.*, 2019, **116**, 9245–9250.
4 X. Leng, X. Hu, W. Zhao, B. An, X. Zhou and Z. Liu, *Adv. Intell. Syst.*, 2021, **3**, 2000185.
5 J. K. Gansel, M. Thiel, M. S. Rill, M. Decker, K. Bade, V. Saile, G. Von Freymann, S. Linden and M. Wegener, *Science*, 2009, **325**, 1513–1515.
6 Y. Yu, F. Fu, L. Shang, Y. Cheng, Z. Gu and Y. Zhao, *Adv. Mater.*, 2017, **29**, 1605765.
7 H. Yang and M. Guo, *Macromol. Rapid Commun.*, 2019, **40**, 1900111.
8 T. Lin, H. Wang and X. Wang, *Adv. Mater.*, 2005, **17**, 2699–2703.
9 S. Chen, H. Hou, P. Hu, J. H. Wendorff, A. Greiner and S. Agarwal, *Macromol. Mater. Eng.*, 2009, **294**, 781–786.
10 S. Chen, H. Hou, P. Hu, J. H. Wendorff, A. Greiner and S. Agarwal, *Macromol. Mater. Eng.*, 2009, **294**, 265–271.
11 T. Zhao, Y. Zheng and Y. Zeng, *J. Polym. Sci., Part B: Polym. Phys.*, 2019, **57**, 1496–1505.
12 W. Wang, A. Saeed, J. He, Z. Wang, D. Zhan, Z. Li, C. Wang, Y. Sun, F. Tao and W. Xu, *J. Colloid Interface Sci.*, 2020, **578**, 304–314.
13 P. Liu, Y. Li, Y. Xu, L. Bao, L. Wang, J. Pan, Z. Zhang, X. Sun and H. Peng, *Small*, 2018, **14**, 1702926.
14 A. Mishra, Y. Loo, R. Deng, Y. J. Chuah, H. T. Hee, J. Y. Ying and C. A. E. Hauser, *Nano Today*, 2011, **6**, 232–239.
15 L. Dai, J. You, W. Shen, K.-D. Zhu and X. Huang, *Mater. Des.*, 2023, **226**, 111623.
16 J. Shi, S. Liu, L. Zhang, B. Yang, L. Shu, Y. Yang, M. Ren, Y. Wang, J. Chen, W. Chen, Y. Chai and X. Tao, *Adv. Mater.*, 2020, **32**, 1901958.
17 J. Woo, H. Lee, C. Yi, J. Lee, C. Won, S. Oh, J. Jekal, C. Kwon, S. Lee, J. Song, B. Choi, K. Jang and T. Lee, *Adv. Funct. Mater.*, 2020, **30**, 1910026.
18 S. Kato, D. W. Carlson, A. Q. Shen and Y. Guo, *Microsyst. Nanoeng.*, 2024, **10**, 1–10.
19 L. Wei, S. Wang, M. Shan, Y. Li, Y. Wang, F. Wang, L. Wang and J. Mao, *Bioactive Mater.*, 2023, **22**, 343–364.
20 C. Xu, Z. Jiang, T. Zhong, C. Chen, W. Ren, T. Sun and F. Fu, *ACS Omega*, 2023, **8**, 2243–2252.
21 H. S. Hwang, H. J. Jung, J. G. Kim, H. S. Jeong, W. J. Lee and S. O. Kim, *Adv. Funct. Mater.*, 2023, **33**, 2212997.
22 H. Yao, H. Zhang and H. Zheng, *ChemCatChem*, 2024, e202400177.
23 C. Mu, T. Zhu, Y. Zhou, Y. Gu, Q. Yang and B. Wu, *Colloids Surf., A*, 2024, **683**, 132977.
24 G. Shao, C. Su, C. Shi, Z. Xu, M. Ye, N. Chen, R. Yu and X. Y. Liu, *Electrochim. Acta*, 2022, **404**, 139611.
25 F. Sheng, B. Zhang, Y. Zhang, Y. Li, R. Cheng, C. Wei, C. Ning, K. Dong and Z. L. Wang, *ACS Nano*, 2022, **16**, 10958–10967.
26 Q. Xia, L. Meng, T. He, G. Huang, B. S. Li and B. Z. Tang, *ACS Nano*, 2021, **15**, 4956–4966.
27 W. Ma, S. Ling, J. Zhang, Z. Chen and J. Xu, *J. Polym. Sci.*, 2022, **60**, 1741–1749.
28 S. M. Hosseini, M. Ghiaci, S. A. Kulinich, W. Wunderlich, H. S. Ghaziaskar and A. J. Koupaei, *Appl. Catal., A*, 2022, **630**, 118456.
29 Q. Liang, J. Wan, P. Ji, D. Zhang, N. Sheng, S. Chen and H. Wang, *Chem. Eng. J.*, 2022, **427**, 131904.
30 Y. Chen, X. Tang, J. Zhong, J. Li, M. Li and T. Zhang, *Appl. Surf. Sci.*, 2022, **578**, 152122.
31 Q. Liang, D. Zhang, T. He, Z. Zhang, Y. Wu, G. Zhang, R. Xie, S. Chen, H. Wang and C. Lee, *Nano Energy*, 2023, **117**, 108903.
32 H. Ma, X. Zhang, Z. Zhang, Y. Wang, G. Wang, F. Liu, R. Cui, C. Huang, M. Wang, Y. Wei, K. Jiang, L. Pan and K. Liu, *J. Mater. Chem. C*, 2019, **7**, 12095–12103.
33 N. Tang, W. Kuo, C. Jeng, L. Wang, K. Lin and Y. Du, *ACS Nano*, 2010, **4**, 781–788.
34 D. Xu, C. Xuan, X. Li, Z. Luo, Z. Wang, T. Tang, J. Wen, M. Li and J. Xiao, *Electrochim. Acta*, 2020, **339**, 135912.
35 Y. Han, C. Jiang, H. Lin, C. Luo, R. Qi and H. Peng, *Energy Technol.*, 2020, **8**, 1901249.
36 G. M. Spinks, *Adv. Mater.*, 2020, **32**, 1904093.
37 H.-W. Huang, M. S. Sakar, A. J. Petruska, S. Pané and B. J. Nelson, *Nat. Commun.*, 2016, **7**, 12263.
38 L. Huang, X. Xie, H. Huang, J. Zhu, J. Yu, Y. Wang and Z. Hu, *Sens. Actuators, A*, 2020, **302**, 111793.
39 J. J. Wie, M. R. Shankar and T. J. White, *Nat. Commun.*, 2016, **7**, 13260.
40 Y. Wei, H. Huo, C. Huang, Q. Zhang, R. Hoogenboom and F. Liu, *Eur. Polym. J.*, 2020, **125**, 109537.
41 Q. Qu, A. Yang, J. Wang, M. Xie, X. Zhang, D. Huang, R. Xiong, D. Pei and C. Huang, *J. Colloid Interface Sci.*, 2023, **649**, 68–75.
42 S. Gao, A. Zhou, B. Cao, J. Wang, F. Li, G. Tang, Z. Jiang, A. Yang, R. Xiong, J. Lei and C. Huang, *New J. Chem.*, 2021, **45**, 13056–13063.
43 X. Wei, Y. Xue, Y. Sun, L. Chen, C. Zhang, Q. Wu, S. Peng, C. Ma, Z. Liu, S. Jiang, X. Yang, S. Agarwal and G. Duan, *Chem. Eng. J.*, 2023, **452**, 139373.
44 L. Chen, Y. Zhang, K. Zhang, F. Li, G. Duan, Y. Sun, X. Wei, X. Yang, F. Wang, C. Zhang, S. Li, X. Cao, C. Ma and S. Jiang, *Chem. Eng. J.*, 2024, **480**, 148205.
45 K. M. Lee, T. J. Bunning and T. J. White, *Adv. Mater.*, 2012, **24**, 2839–2843.
46 K. M. Lee, M. L. Smith, H. Koerner, N. Tabiryan, R. A. Vaia, T. J. Bunning and T. J. White, *Adv. Funct. Mater.*, 2011, **21**, 2913–2918.

47 X. Zhang, L. Li, Y. Chen, C. Valenzuela, Y. Liu, Y. Yang, Y. Feng, L. Wang and W. Feng, *Angew. Chem.*, 2024, **136**, e202404202.
48 H. L. Gao, R. Zhao, C. Cui, Y. B. Zhu, S. M. Chen, Z. Pan, Y. F. Meng, S. M. Wen, C. Liu, H. A. Wu and S. H. Yu, *Natl. Sci. Rev.*, 2020, **7**, 73–83.
49 C. Li, J. Wang and B. Zhang, *J. Appl. Polym. Sci.*, 2012, **123**, 2992–2995.
50 M. Wang, Z. Chen, L. Dong, J. Wu, C. Li, Q. Gao, J. Shi, C. Zhu and H. Morikawa, *Chem. Eng. J.*, 2023, **457**, 141164.
51 J. Feng, *Mater. Lett.*, 2017, **189**, 180–183.
52 X. Zhang, J. Chen and Y. Zeng, *Polymer*, 2020, **201**, 122609.
53 T. Zhao, Y. Xu, M. Wu, Y. Li, J. Ma, H. Li, Y. Zheng and Y. Zeng, *Nano Lett.*, 2024, **24**, 1385–1391.
54 S. Cai, R. Liu, H. He and X. Ning, *Mater. Lett.*, 2023, **351**, 135063.
55 R. Liu, B. Kong, Y. Chen, X. Liu and S. Mi, *Sens. Actuators, B*, 2020, **304**, 127069.
56 W. Ma, Y. Liu, S. Ling, Z. Chen and J. Xu, *Chem. Eng. Sci.*, 2023, **282**, 119339.
57 Y. Qin, Z. Zhang and Z. Cui, *Carbon*, 2004, **42**, 1917–1922.
58 X. Jian, M. Jiang, Z. Zhou, M. Yang, J. Lu, S. Hu, Y. Wang and D. Hui, *Carbon*, 2010, **48**, 4535–4541.
59 H. Cui, X. Chen, Y. Wang, D. Wei, F. Qiu and J. Peng, *Soft Matter*, 2018, **14**, 5906–5912.
60 I. Danila, F. Riobé, F. Piron, J. Puigmartí-Luis, J.-D. Wallis, M. Linares, H. Ågren, D. Beljonne, D. B. Ama-bilino and N. Avarvari, *J. Am. Chem. Soc.*, 2011, **133**, 8344–8353.
61 A. R. A. Palmans, J. A. J. M. Vekemans, H. Fischer, R. A. Hikmet and E. W. Meijer, *Chem. – Eur. J.*, 1997, **3**, 300–307.
62 X. Xu, Y. Xie, P. Guo, Y. Shi, M. Sun, J. Zhou, C. Wang, C. Han, J. Liu and T. Li, *Food Chem.*, 2023, **404**, 134645.
63 J. He, J. He, X. Xu, B. Du, B. Xu, C. Liao, Z. Bai and Y. Wang, *Photon. Res.*, 2021, **9**, 2052–2059.
64 J. Y. Han, K. Kim, C. Lee and D. K. Yoon, *Macromol. Rapid Commun.*, 2023, 2300303.
65 D. Brüggemann, J. Michel, N. Suter, M. G. de Aguiar and M. Maas, *J. Nanotechnol.*, 2020, **11**, 991–999.
66 C. J. Tan, J. J. L. Lee, B. C. Ang, A. Andriyana, G. Chagnon and M. S. Sukiman, *J. Appl. Polym. Sci.*, 2019, **136**, 47706.
67 A. AlAttar, E. Gkouti and A. Czekanski, *J. Mech. Behav. Biomed. Mater.*, 2023, **147**, 106157.
68 G. Zhao, T. Wu, R. Wang, Z. Li, Q. Yang, L. Wang, H. Zhou, B. Jin, H. Liu, Y. Fang, D. Wang and F. Xu, *Sci. Adv.*, 2023, **9**, eadj5407.
69 W. Zhang, J. Miao, M. Tian, X. Zhang, T. Fan and L. Qu, *Chem. Eng. J.*, 2023, **462**, 142279.
70 Y. Zhang, H. Yu, Q. Qin, C. Qu and J. Wang, *Acta Mech. Sin.*, 2023, **39**, 622403.
71 Z. Hu, Y. Zhang, H. Jiang and J. Lv, *Sci. Adv.*, 2023, **9**, eadh3350.
72 J. Cui, T. Lu, F. Li, Y. Wang, J. Lei, W. Ma, Y. Zou and C. Huang, *J. Colloid Interface Sci.*, 2021, **582**, 506–514.
73 Y. Deng, T. Lu, J. Cui, S. Keshari Samal, R. Xiong and C. Huang, *Sep. Purif. Technol.*, 2021, **277**, 119623.
74 J. Cui, Y. Wang, T. Lu, K. Liu and C. Huang, *J. Colloid Interface Sci.*, 2021, **597**, 48–55.
75 Y. Deng, T. Lu, J. Cui, W. Ma, Q. Qu, X. Zhang, Y. Zhang, M. Zhu, R. Xiong and C. Huang, *Sep. Purif. Technol.*, 2022, **294**, 121093.
76 X. Wei, Q. Wu, L. Chen, Y. Sun, L. Chen, C. Zhang, S. Li, C. Ma and S. Jiang, *ACS Appl. Mater. Interfaces*, 2023, **15**, 10030–10043.
77 X. Wei, L. Chen, Y. Wang, Y. Sun, C. Ma, X. Yang, S. Jiang and G. Duan, *Chem. Eng. J.*, 2022, **433**, 134258.
78 W. Cao, W. Ma, T. Lu, Z. Jiang, R. Xiong and C. Huang, *J. Colloid Interface Sci.*, 2022, **608**, 164–174.
79 J. Cui, F. Li, Y. Wang, Q. Zhang, W. Ma and C. Huang, *Sep. Purif. Technol.*, 2020, **250**, 117116.
80 W. Cao, M. Zhang, W. Ma and C. Huang, *Sep. Purif. Technol.*, 2023, **327**, 124952.
81 W. Ma, Y. Ding, Y. Li, S. Gao, Z. Jiang, J. Cui, C. Huang and G. Fu, *J. Membr. Sci.*, 2021, **634**, 119402.
82 H. Guo, Y. Chen, Y. Li, W. Zhou, W. Xu, L. Pang, X. Fan and S. Jiang, *Composites, Part A*, 2021, **143**, 106309.
83 H. Guo, Y. Li, Y. Ji, Y. Chen, K. Liu, B. Shen, S. He, G. Duan, J. Han and S. Jiang, *Compos. Commun.*, 2021, **27**, 100879.
84 H. Guo, F. Wang, H. Luo, Y. Li, Z. Lou, Y. Ji, X. Liu, B. Shen, Y. Peng, K. Liu and S. Jiang, *Composites, Part A*, 2021, **151**, 106662.
85 P. E. S. Silva, F. Vistulo De Abreu and M. H. Godinho, *Soft Matter*, 2017, **13**, 6678–6688.
86 S. Motojima, I. Hasixgawa, S. Kagiya, K. Andoh and H. Iwanaga, *Carbon*, 1995, **33**, 1167–1173.
87 Y. Li, T. Zhao, Y. Xu, X. Zhang, X. Chen and Y. Zeng, *Fibers Polym.*, 2024, **25**, 693–701.
88 T. Zhao, Y. Zheng, X. Zhang, D. Teng, Y. Xu and Y. Zeng, *Mater. Des.*, 2021, **205**, 109705.
89 H. Li, H. Huang, X. Meng and Y. Zeng, *J. Polym. Sci., Part B: Polym. Phys.*, 2018, **56**, 970–977.
90 G. Sun, W. Han, Y. Wang, S. Xin, J. Yang, F. Zou, X. Wang and C. Xiao, *Ind. Eng. Chem. Res.*, 2022, **61**, 1004–1021.
91 Y. Zhao, D. Dong, Y. Wang, S. Gong, T. An, L. W. Yap and W. Cheng, *ACS Appl. Mater. Interfaces*, 2018, **10**, 42612–42620.
92 T. Luelf, C. Bremer and M. Wessling, *J. Membr. Sci.*, 2016, **506**, 86–94.
93 H. Yücel and P. Z. Çulfaz-Emecen, *J. Membr. Sci.*, 2018, **559**, 54–62.
94 N. M. Ribe, *Proc. R. Soc. London, Ser. A*, 2004, **460**, 3223–3239.
95 K. Sugiyasu, S. Tamaru, M. Takeuchi, D. Berthier, I. Huc, R. Oda and S. Shinkai, *Chem. Commun.*, 2002, 1212–1213.
96 W.-J. Kim and S.-M. Yang, *Adv. Mater.*, 2001, **13**, 1191–1195.
97 X. Xu, Y. Zuo, S. Cai, X. Tao, Z. Zhang, X. Zhou, S. He, X. Fang and H. Peng, *J. Mater. Chem. C*, 2018, **6**, 4866–4872.
98 K. Akagi, *Chem. Rev.*, 2009, **109**, 5354–5401.
99 H. Niu, H. Zhang, W. Yue, S. Gao, H. Kan, C. Zhang, C. Zhang, J. Pang, Z. Lou, L. Wang, Y. Li, H. Liu and G. Shen, *Small*, 2021, **17**, 2100804.
100 L. Shang, Y. Cheng and Y. Zhao, *Chem. Rev.*, 2017, **117**, 7964–8040.
101 S. Motojima, Y. Itoh, S. Asakura and H. Iwanaga, *J. Mater. Sci.*, 1995, **30**, 5049–5055.

102 M. Tao, G. Du, T. Yang, W. Gao, L. Zhang, W. Du, J. Jiang, S. Bao and M. Xu, *J. Mater. Chem. A*, 2020, **8**, 3018–3026.
103 Y. Yue, Y. Wang, X. Xu, C. Wang, Z. Yao and D. Liu, *Ceram. Int.*, 2022, **48**, 6338–6346.
104 B. S. Li, R. Wen, S. Xue, L. Shi, Z. Tang, Z. Wang and B. Z. Tang, *Mater. Chem. Front.*, 2017, **1**, 646–653.
105 T. Li, J. Li, Z. Xu, Y. Tian, J. Li, J. Du and F. Meng, *Small*, 2023, **19**, 2300233.
106 R. Zhong, Q. Tang, S. Wang, H. Zhang, F. Zhang, M. Xiao, T. Man, X. Qu, L. Li, W. Zhang and H. Pei, *Adv. Mater.*, 2018, **30**, 1706887.
107 H. Li, X. Zheng, H. Su, J. W. Y. Lam, K. Sing Wong, S. Xue, X. Huang, X. Huang, B. S. Li and B. Z. Tang, *Sci. Rep.*, 2016, **6**, 19277.
108 L. Zhang, Y. B. Zhu, C. L. Ge, C. Wei and Q. L. Wang, *Solid State Commun.*, 2007, **142**, 541–544.
109 L. Wang, C. Li, F. Gu and C. Zhang, *J. Alloys Compd.*, 2009, **473**, 351–355.
110 G. Arrachart, C. Carcel, P. Trens, J. J. E. Moreau and M. Wong Chi Man, *Chem. - Eur. J.*, 2009, **15**, 6279–6288.
111 D. Luo, A. Maheshwari, A. Danielescu, J. Li, Y. Yang, Y. Tao, L. Sun, D. K. Patel, G. Wang, S. Yang, T. Zhang and L. Yao, *Nature*, 2023, **614**, 463–470.
112 F. Zhou and R. Gong, *Polym. Int.*, 2008, **57**, 837–845.
113 A. Rohani Shirvan, A. Nouri and A. Sutti, *Eur. Polym. J.*, 2022, **181**, 111681.
114 J. Cheng, Y. Jun, J. Qin and S.-H. Lee, *Biomaterials*, 2017, **114**, 121–143.
115 S. Boonyod, W. Pivsa-Art and S. Pivsa-Art, *Fibers Polym.*, 2022, **23**, 1525–1531.
116 D. Bokov, A. Turki Jalil, S. Chupradit, W. Suksatan, M. Javed Ansari, I. H. Shewael, G. H. Valiev and E. Kianfar, *Adv. Mater. Sci. Eng.*, 2021, 1–21.
117 W. Zhang, R. Cheng, H. Bi, Y. Lu, L. Ma and X. He, *New Carbon Mater.*, 2021, **36**, 69–81.
118 M. Zhang, X. Peng, P. Fan, Y. Zhou and P. Xiao, *Macromol. Chem. Phys.*, 2022, **223**, 2100451.
119 Y. Manawi Ihsanullah, A. Samara, T. Al-Ansari and M. Atieh, *Materials*, 2018, **11**, 822.
120 S. Won, S. Kim, J. E. Park, J. Jeon and J. J. Wie, *Nat. Commun.*, 2019, **10**, 4751.
121 C. Sun, J. Luo, S. Yan, K. Li, Y. Li, H. Wang, C. Hou and Q. Zhang, *Adv. Funct. Mater.*, 2023, **33**, 2211035.
122 S. Iamsaard, S. J. Aßhoff, B. Matt, T. Kudernac, J. J. L. M. Cornelissen, S. P. Fletcher and N. Katsonis, *Nat. Chem.*, 2014, **6**, 229–235.
123 A. A. Ashkarran, A. Iraji Zad, S. M. Mahdavi and M. M. Ahadian, *Mater. Chem. Phys.*, 2009, **118**, 6–8.
124 H. Vahabi, H. Wu, M. R. Saeb, J. H. Koo and S. Ramakrishna, *Polymer*, 2021, **217**, 123466.
125 W.-Q. Chen, Q.-T. Li, P.-H. Li, Q.-Y. Zhang, Z.-S. Xu, P. K. Chu, X.-B. Wang and C.-F. Yi, *J. Mater. Sci.*, 2015, **50**, 3860–3874.
126 M. Zhang and A. A. Ogale, *Carbon*, 2014, **69**, 626–629.
127 X. Mei, X. Meng and F. Wu, *Phys. E*, 2015, **68**, 81–86.
128 X. Ding and J. M. Selig, *Chin. J. Mech. Eng.*, 2002, **15**, 293–297.
129 J. Park, M. Park, G. Nam, J. S. Lee and J. Cho, *Adv. Mater.*, 2014, **27**, 1396–1401.
130 A. M. Zamarayeva, A. E. Ostfeld, M. Wang, J. K. Duey, I. Deckman, B. P. Lechêne, G. Davies, D. A. Steingart and A. C. Arias, *Sci. Adv.*, 2017, **3**, e1602051.
131 K. Liu, B. Kong, W. Liu, Y. Sun, M.-S. Song, J. Chen, Y. Liu, D. Lin, A. Pei and Y. Cui, *Joule*, 2018, **2**, 1857–1865.
132 D. Zhang, W. Yang, W. Gong, W. Ma, C. Hou, Y. Li, Q. Zhang and H. Wang, *Adv. Mater.*, 2021, **33**, 2100782.
133 L. Lao, D. Shou, Y. S. Wu and J. T. Fan, *Sci. Adv.*, 2020, **6**, eaaz0013.
134 X. Zhang, W. Yang, Z. Shao, Y. Li, Y. Su, Q. Zhang, C. Hou and H. Wang, *ACS Nano*, 2022, **16**, 2188–2197.
135 Q. Gao, Z. Chen, C. Liu, Y. Wang, J. Zhu and C. Gao, *J. Alloys Compd.*, 2024, **980**, 173547.
136 B. Yu, Q. Gu, G. Hu, T. Yang, M. Liu, H. Shi, Z. Xiang, T. Huang, M. Zhu and H. Yu, *Chem. Eng. J.*, 2024, **480**, 148058.
137 Y. Lu, B. Li, Z. Zhang, R. Gao, J. Xiong, F. Guo and Y. Zhao, *Adv. Electron. Mater.*, 2024, 2400059.
138 W. Ma, D. Liu, S. Ling, J. Zhang, Z. Chen, Y. Lu and J. Xu, *ACS Appl. Mater. Interfaces*, 2021, **13**, 59392–59399.
139 Q. Liang, D. Zhang, P. Ji, N. Sheng, M. Zhang, Z. Wu, S. Chen and H. Wang, *ACS Appl. Mater. Interfaces*, 2021, **13**, 1545–1554.
140 M. Zhang, S. Chen, N. Sheng, B. Wang, J. Yao, Z. Wua and H. Wang, *Nanoscale*, 2019, **11**, 15347–15358.
141 Y. Gao, F. Guo, P. Cao, J. Liu, D. Li, J. Wu, N. Wang, Y. Su and Y. Zhao, *ACS Nano*, 2020, **14**, 3442–3450.
142 K. Suzuki, K. Yataka, Y. Okumiya, S. Sakakibara, K. Sako, H. Mimura and Y. Inoue, *ACS Sens.*, 2016, **1**, 817–825.
143 S. Wang, P. Xiao, Y. Liang, J. Zhang, Y. Huang, S. Wu, S.-W. Kuo and T. Chen, *J. Mater. Chem. C*, 2018, **6**, 5140–5147.
144 Y. Ling, W. Pang, J. Liu, M. Page, Y. Xu, G. Zhao, D. Stalla, J. Xie, Y. Zhang and Z. Yan, *Nat. Commun.*, 2022, **13**, 524.
145 D.-C. Wang, Y. Lei, W. Jiao, Y.-F. Liu, C.-H. Mu and X. Jian, *Rare Met.*, 2021, **40**, 3–19.
146 S. Liu, Y. Chen, Z. Zhu, E. Ren, J. Wang, Y. Wang, J. Qin and P. Cheng, *Polymer*, 2024, 127072.
147 T. Klotz, R. Pothier, D. Walch and T. Colombo, *Results Eng.*, 2021, **9**, 100190.
148 P. Jousset, T. Reinsch, T. Ryberg, H. Blanck, A. Clarke, R. Aghayev, G. P. Hersir, J. Henninges, M. Weber and C. M. Krawczyk, *Nat. Commun.*, 2018, **9**, 5114.
149 H. Bai, S. Li, J. Barreiros, Y. Tu, C. R. Pollock and R. F. Shepherd, *Science*, 2020, **370**, 848–852.
150 Z. Song, Y. Li and J. Hu, *Sensors*, 2023, **23**, 2874.
151 W. Chang, Z. Shi, X. Wang, P. Wang, Z. Wang and Y.-G. Liu, *Opt. Express*, 2023, **31**, 30470.
152 J. J. Giner-Casares and L. M. Liz-Marzán, *Nano Today*, 2014, **9**, 365–377.
153 J. Kumar, H. Eraña, E. López-Martínez, N. Claes, V. F. Martín, D. M. Solís, S. Bals, A. L. Cortajarena, J. Castilla and L. M. Liz-Marzán, *Proc. Natl. Acad. Sci. U. S. A.*, 2018, **115**, 3225–3230.
154 D. N. Woolfson, *Biopolymers*, 2010, **94**, 118–127.
155 C. Gribbon, K. J. Channon, W. Zhang, E. F. Banwell, E. H. C. Bromley, J. B. Chaudhuri, R. O. C. Oreffo and D. N. Woolfson, *Biochemistry*, 2008, **47**, 10365–10371.
156 G. Chang and J. Shen, *Macromol. Rapid Commun.*, 2010, **31**, 2151–2154.

157 X. Hu, L. Yang, Y. Zhang, B. Shou, H.-T. Ren, J.-H. Lin, C.-W. Lou and T.-T. Li, *Int. J. Biol. Macromol.*, 2023, **253**, 126737.
158 L. Wang, H. Jiang, F. Wan, H. Sun, Y. Yang, W. Li, Z. Qian, X. Sun, P. Chen, S. Chen and H. Peng, *Adv Healthcare Mater.*, 2023, 2301610.
159 X. Zhang, Y. Luan, Y. Li, Z. Wang, Z. Li, F. Xu and Z. Guo, *Compos. Struct.*, 2021, **276**, 114575.
160 Y. Zou, Y. Gai, P. Tan, D. Jiang, X. Qu, J. Xue, H. Ouyang, B. Shi, L. Li, D. Luo, Y. Deng, Z. Li and Z. L. Wang, *Fundam. Res.*, 2022, **2**, 619–628.
161 C. Wang, Y. Liu, X. Qu, B. Shi, Q. Zheng, X. Lin, S. Chao, C. Wang, J. Zhou, Y. Sun, G. Mao and Z. Li, *Adv. Mater.*, 2022, **34**, 2105416.
162 E. Pasquier, R. Skunde and J. Ruwoldt, *J. Bioresour. Bioprod.*, 2023, **8**, 408–420.
163 Y. Zhang, Y. Zhao, Y. Wu, B. Zhao, L. Wang, B. Song and C. Huang, *Spectrochim. Acta, Part A*, 2021, **247**, 119123.
164 H. Ma, Z. Cheng, X. Li, B. Li, Y. Fu and J. Jiang, *J. Bioresour. Bioprod.*, 2023, **8**, 15–32.
165 Y. Zhang, Y. Zhao, A. Zhou, Q. Qu, X. Zhang, B. Song, K. Liu, R. Xiong and C. Huang, *Spectrochim. Acta, Part A*, 2021, **261**, 120014.
166 D. Li, T. Cui, J. Jian, J. Yan, J. Xu, X. Li, Z. Li, A. Yan, Z. Chen, W. Shao, Z. Tang, Z. Xu, G. Wu, H. Liu, Y. Yang and T. Ren, *Adv. Funct. Mater.*, 2023, **33**, 2213335.
167 Q. Liang, D. Zhang, Y. Wu, X. Qu, Y. Jia, S. Chen, H. Wang and C. Lee, *Nano Energy*, 2023, **113**, 108598.
168 P. S. Goh, W. J. Lau, M. H. D. Othman and A. F. Ismail, *Desalination*, 2018, **425**, 130–155.
169 S. Kerdi, A. Qamar, A. Alpatova, J. S. Vrouwenvelder and N. Ghaffour, *Desalination*, 2020, **484**, 114454.
170 A. Zrelli, J. Debaya, A. Doucoure and B. Chaouachi, *ETJ*, 2022, **41**, 1–11.
171 M. Yang, Y. Xu, X. Zhang, H. K. Bisoyi, P. Xue, Y. Yang, X. Yang, C. Valenzuela, Y. Chen, L. Wang, W. Feng and Q. Li, *Adv. Funct. Mater.*, 2022, **32**, 2201884.
172 I. Fiorello, E. Del Dottore, F. Tramacere and B. Mazzolai, *Bioinspiration Biomimetics*, 2020, **15**, 031001.
173 F. Meder, S. P. Murali Babu and B. Mazzolai, *IEEE Robot. Autom. Lett.*, 2022, **7**, 5191–5197.
174 M. Yang, L. P. Cooper, N. Liu, X. Wang and M. P. Fok, *Opt. Express*, 2020, **28**, 35158.
175 B. Yigit, Y. Alapan and M. Sitti, *Adv. Sci.*, 2019, **6**, 1801837.
176 Z. Bazrafshan and G. K. Stylios, *Int. J. Biol. Macromol.*, 2019, **129**, 693–705.
177 X. Chen, K. Wu, Y. Zhang, D. Liu, R. Li and Q. Fu, *Adv. Mater.*, 2022, **34**, 2206088.
178 X. Chen, K. Wu, Y. Zhang, D. Liu, R. Li and Q. Fu, *Adv. Mater.*, 2022, **34**, 2206088.
179 N. Kharouf, S. Sauro, L. Hardan, H. Jmal, G. Bachagha, V. Macaluso, F. Addiego, F. Inchingolo, Y. Haikel and D. Mancino, *JCM*, 2022, **11**, 6754.
180 D. Feng, Y. Xiao, G. Wang, G. Mei, W. Guo, K. Yu, S. Liu, W. Zhao, X. Zhou and Z. Liu, *Macromol. Rapid Commun.*, 2023, **44**, 2300318.
181 Z. Wang and R. H. Baughman, *J. Compos. Mater.*, 2023, **57**, 805–815.
182 Y. Zhang, H. Xiao, R. Xiong and C. Huang, *Sep. Purif. Technol.*, 2023, **324**, 124513.
183 J. Wei, H. Huo, H. Hou, C. Chen, S. Wang and D. Min, *J. For. Eng.*, 2022, **7**, 107–113.
184 T. Lu, W. Cao, H. Liang, Y. Deng, Y. Zhang, M. Zhu, W. Ma, R. Xiong and C. Huang, *Langmuir*, 2022, **38**, 15729–15739.
185 H. S. Shahraki, R. Bushra, N. Shakeel, A. Ahmad Quratulen, M. Ahmad and C. Ritzoulis, *J. Bioresour. Bioprod.*, 2023, **8**, 162–175.
186 J. Cao, W. He, P. Zhou, B. Wei, R. Wang, S. Liang and Q. Ji, *J. For. Eng.*, 2023, **8**, 113–120.
187 T. N. Karunaratne, P. M. Rodrigo, D. O. Oguntuyi, T. E. Mlsna, J. Zhang and X. Zhang, *J. Bioresour. Bioprod.*, 2023, **8**, 388–398.
188 S. Jiang, H. Liu, W. Zhang and Y. Lu, *Bioresour. Technol.*, 2024, **405**, 130936.
189 T. Lu, H. Liang, W. Cao, Y. Deng, Q. Qu, W. Ma, R. Xiong and C. Huang, *J. Colloid Interface Sci.*, 2022, **608**, 2860–2869.
190 Y. Yu, X. Wei, W. Chen, G. Qian, C. Chen, S. Wang and D. Min, *ChemSusChem*, 2024, **17**, e202301105.
191 T. Lu, H. Liang, W. Cao, Y. Deng, Q. Qu, W. Ma, R. Xiong and C. Huang, *J. Colloid Interface Sci.*, 2022, **608**, 2860–2869.
192 F. Liu, Y. Liu, D. Jiang, R. Zhang, Y. Cui and M. Li, *Ecotoxicology*, 2014, **23**, 567–576.
193 K. Hou, J. Wang and H. Li, *Rapid Commun. Mass Spectrom.*, 2007, **21**, 3554–3560.
194 C. Wu, W. Liu, J. Jiang, Y. Wang, K. Hou and H. Li, *Talanta*, 2019, **192**, 46–51.
195 J. Zhang, Q. Lu, R. Ni, Y. Shi, S. Duan, J. Ma, Y. Hu, W. Hu, Q. Ke and Y. Zhao, *Int. J. Biol. Macromol.*, 2023, **245**, 125512.
196 J. Yan, J. Liu, H. Lei, Y. Kang, C. Zhao and Y. Fang, *J. Colloid Interface Sci.*, 2015, **448**, 374–379.
197 S. Zhu, Z. Wang, X. Liu, Q. Cao, Y. Wen, R. Cao, Z. Wu, C. Zhou, Y. Jin and F. Tao, *Ionics*, 2022, **28**, 1129–1141.
198 S. Xie, Z. Ji, B. Li, L. Zhu and J. Wang, *Composites, Part A*, 2018, **114**, 360–367.
199 L. Huang, Y. Duan, Y. Shi, X. Ma, H. Pang, Q. Zeng and R. Che, *Adv. Opt. Mater.*, 2022, **10**, 2200249.
200 H. Ren, T. Li, H. Wang, Z. Guo, T. Chen and F. Meng, *Chem. Eng. J.*, 2022, **427**, 131582.
201 X. Li, L. Yu, L. Yu, Y. Dong, Q. Gao, Q. Yang, W. Yang, Y. Zhu and Y. Fu, *Chem. Eng. J.*, 2018, **352**, 745–755.
202 X. Zhao, F. Li, H. Guo, W. Cui, X. Sun, R. Wang, X. Jin, Y. Liu, J. He and D. Ji, *ACS Appl. Polym. Mater.*, 2024, **6**, 2983–2992.
203 Y. Yang, X. Zhang, C. Valenzuela, R. Bi, Y. Chen, Y. Liu, C. Zhang, W. Li, L. Wang and W. Feng, *Matter*, 2024, **7**, 2091–2107.
204 Y. Yang, X. Zhang, C. Valenzuela, R. Bi, Y. Chen, Y. Liu, C. Zhang, W. Li, L. Wang and W. Feng, *Matter*, 2024, **7**, 2091–2107.
205 Y. Chen, C. Valenzuela, X. Zhang, X. Yang, L. Wang and W. Feng, *Nat. Commun.*, 2023, **14**, 3036.